Fast Timing in Medical Imaging

P. Lecoq, *Fellow, IEEE,* A.J. Gonzalez, *Member, IEEE*, E. Auffray, *Member, IEEE*, G. Konstantinou, J. Nuyts, *Fellow, IEEE,* J.O. Prior, *Senior Member, IEEE* , R. M. Turtos, J. Varela

Abstract— **We report in this paper on the Fast Timing in Medical Imaging workshop, (Valencia, Jun2 2022). The workshop gathered 104 attendees from all over the world, with representatives from the academic and industrial sectors. During three very dense days, nuclear medicine physicians, radiologists, oncologists, immunologists and biologists have debated with physicists, engineers, technologists of different disciplines, as well as with medical imaging industry representatives to devise about the importance of improving the timing performance of a new generation of medical imaging instrumentation, with a special focus on PET scanners toward the ultimate goal of 10 ps coincidence time resolution (CTR), allowing a millimeter 3D spatial resolution on an event-to-event basis by Time-of-Flight (TOF) techniques.**
This paper summarizes the most up-to-date developments on the roadmap towards the 10ps time of flight challenge based on the contributions to this workshop.
.

Index Terms—
Medical imaging, Scintillators, metascintillator, scintillator heterostructure, PET, Time-of-Flight, photodetector, electronics, image reconstruction.

I. INTRODUCTION

In the recent years, medical imaging has become central in medicine. The progress in the performance of conventional medical imaging modalities as well as the appearance of new modalities have been impressive.

However, a number of new medical challenges call for further technological improvements, in particular in the sensitivity of these devices. These concern new treatment opportunities in the context of personalized (also called precision) medicine, such as the rapid development of cancer immunotherapy and stem cell-based tissue repair procedures, which require *in vivo* tracking of a small number of cells to follow quantitatively and dynamically their biodistribution, differentiation and activity in the patient.

In this regard, Positron Emission Tomography (PET) offers already a high sensitivity at the picomolar level. But the clinical demand is pushing for gaining one or two orders of magnitude. One of the ways of boosting sensitivity is including high precision time-of-flight (TOF) techniques, which will provide a better signal-to-noise ratio (SNR) in the image, allowing detecting smaller size tumors together with a better staging of the patients, thus, opening the way to better diagnostic. Moreover, there is an increasing demand for reducing the radioactive doses injected to the patients and shortening scanning times without impairing image quality. A dose reduction by one order of magnitude would allow extending PET protocols much beyond cancer diagnosis, such as inflammation, cardio-vascular disease, sepsis, infectious disease, just to cite a few. Post-injection scans at longer delays would improve the potential of pharmacodynamic and biodistribution studies. Most importantly, a significant dose reduction would potentiate PET protocols for new categories of patients in the pediatric, neonatal and even prenatal domains. Additionally, shortening scanning time may allow reducing motion artifacts and spreading PET imaging to other categories of patients. More details are given in chapter B of ref. [1] and all the references herein.

Significant efforts and progresses are being carried out in the context to improve the timing resolution of molecular imaging scanners well below the current state-of-the-art in commercially available systems that reaches 211 ps [2]. Reaching a timing uncertainty of 100 ps FWHM would further improve the effective sensitivity by a factor 2.1 and by a factor of about 20 when reaching 10 ps [1]. A number of emerging technologies, in particular in the domain of nanophotonics, ultrafast integrated electronics and artificial intelligence, applied to scintillating crystals, photodetectors, data acquisition and image reconstruction offer new perspectives for a breakthrough in medical imaging and for answering these new medical challenges.

The purpose of the workshop was to put in contact top researchers in the field and discuss about the clinical importance and the technical possibilities to further improve the timing performance of PET scanners, in line with the 10 ps

This paper has been submitted on September 11, 2022.
This work did not involve human subjects or animals in its research.
All authors declare that they have no known conflicts of interest in terms of competing financial interests or personal relationships that could have an influence or are relevant to the work reported in this paper.

P. Lecoq is with Multiwave Metacrystal SA, Geneva, Switzerland, the Instituto de Instrumentación para Imagen Molecular, Centro Mixto CSIC—Universitat Politècnica de València, Valencia, Spain, and CERN (European Organization for Nuclear Research), Geneva, Switzerland (e-mail: paul.lecoq@cern.ch)

A.J. Gonzalez is with the Instituto de Instrumentación para Imagen Molecular, Centro Mixto CSIC—Universitat Politècnica de València, 46022 Valencia, Spain

E. Auffray is with EP department, CERN (European Organization of Nuclear Research), Geneva, Switzerland

J. Nuyts is with Nuclear Medicine & Molecular Imaging, MIRC, KU Leuven, Belgium

J. Prior is with Department of Nuclear Medicine and Molecular Imaging, Lausanne University Hospital, Switzerland

J. Varela is with LIP, University of Lisbon, Lisbon, Portugal

Time-of- Flight PET (TOFPET) challenge [3]. A number of sessions attempted to cover as much as possible the different aspects of the problematics of fast timing in medical imaging, with a strong focus on TOFPET, as well as the different elements of harware (scintillators, photodetectors, electronics) but also software (image reconstruction and AI image based processing), summarised in the following sections.

II. CLINICAL MOTIVATIONS FOR PUSHING THE TOFPET COINCIDENCE TIME RESOLUTION (CTR) BELOW 100 PS

This section reports on the introductory session of the workshop, the objective of which, was to review the history of TOF in PET imaging (sub-section A) and to present an overview of the clinical impact of improved PET sensitivity on the basis of the acquired experience and ongoing R&D with state-of-the-art TOFPET, Total Body PET scanners and R&D setups (sub-sections B to E). The potential impact of fast timing in MRI is mentioned is sub-section F.

A. Time-of-Flight in PET imaging, a brief history

As reported by D. Townsend in the introduction to the workshop, the importance of TOF in PET imaging has been recognized as early as in the early 1980's by visionary people like MM. Ter-Pergossian [4], R. Allemand [5], NA Mullani and WH Wong [6], developing the concept of the first TOFPET prototypes using barium fluoride (BaF_2) or cesium fluoride (CsF) fast scintillating crystals. First approaches to evaluate the impact of TOF on the image SNR have been analyzed and formalized by T. Tomitani in 1981 [7] and T. Budinger in 1983 [8].

However, the low sensitivity of the fast scintillators known at that time, namely BaF_2 and CsF, did not allow to take advantage of their sub-ns timing resolution and the TOF approach was abandoned in favor of the much higher sensitivity of the slower BGO crystal. Things changed in the 2000's, with the introduction the LSO crystal, with a detection efficiency nearly as good as BGO but 10 times faster, which triggered again the interest for TOFPET developments. The number of publications on TOFPET has exploded in the last decade (Fig. 1) and steady progress has been made in TOFPET performance, reaching recently a CTR of nearly 200ps at the system level for the Siemens Biograph Vision machine [2].

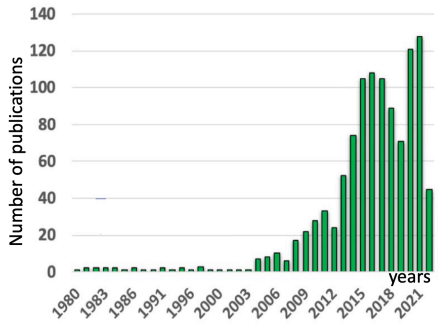

Fig. 1: Publications on TOFPET. Courtesy of D. Townsend.

B. Clinical impact of fast TOFPET

Based on recent literature and clinical experience, a 100 ps TOF-PET introduces a gain in sensitivity versus non-TOF of > 8 (for the center of a uniform cylinder with 20 cm diameter) [1, 2], leading to better lesion detectability, lesion Standardized Uptake Value (SUV) quantification and biomarker distribution (e.g., heterogeneity). This more accurate information would be available for patient management. The gain in effective sensitivity can be used for a much lower scan time for the same injected activity or a much lower injected activity, thus radiation dose for the same acquisition time.

The Lausanne university hospital (CHUV) has acquired a Biograph Vision 600 PET scanner from Siemens three years ago. Prof. John Prior, head of the CHUV nuclear medicine department reported about his experience with this machine in oncology, brain and cardiac imaging. The strong impact of the 211 ps CTR on image quality, allows a systematic reduction of 30% of the scan time and of the injected dose to the patient when TOF information is turned on. It improves the signal recovery and quantification of small structures, as compared to scanners with worse CTR resolution. The SNR improvement in the reconstructed image is particularly significant for imaging structures with low metabolism. Importantly, Prof. John Prior concluded on the basis of his own experience that a more precise definition of the nature of the lesions (oncologic, inflammatory, physiologic), allows a more accurate staging for the therapy management.

Georges El Fakhri from the Gordon Center for Medical Imaging in Boston showed how the progresses in TOFPET performance can contribute to a paradigm shift in medicine, going from the treatment of overt diseases to early diagnosis and prevention. An estimation of the expected performance gain as a function of the TOFPET resolution can be made, based on the Cramer Rao lower bound analysis (CRLB). The principle is to calculate the variance of an unbiased estimator for a given data acquisition strategy, independent of the reconstruction algorithm [9]. Interestingly, the gain is more important for small lesions, low contrast structures and small number of recorded events.

Going from non-TOF to 100 ps TOFPET resolution, the CRLB gain for activity estimation increases from 2.54 to 3.8 when 50 million or 10 million events are recorded respectively. A small contrast of 2:1 leads to a CRLB gain of 7.5, which reduces to 6.5 when the contrast increases to 6:1. Similarly, for the same contrast of 2:1, the CRLB gain increases from 4.0 for a 3.5 cm lesion to 7.4 for a 1 cm lesion.

As shown in [10], an excellent timing resolution can be exploited to simplify the PET design and cost. Indeed, the SNR gain allowed by excellent timing resolution can be exploited to compensate sensitivity losses from reduced or incomplete axial and azimuthal coverage. Moreover, by reducing for each event the number of useful voxels on the line of response of each event, TOF significantly suppresses the artifacts resulting from incomplete tomographic reconstruction. This opens the way to open geometries, particularly useful for on-line monitoring of the radiation distribution in hadrontherapy. This can be also

exploited in the context of Total Body PET imaging, for reducing the number of channels and the cost of PET scanners with a very long axial coverage (Fig. 2).

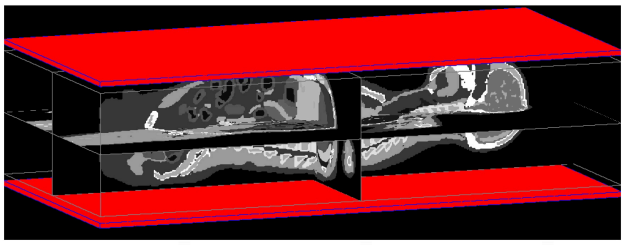

Fig. 2: Flat panel limited angle PET geometry (Gate simulation using the XCAT phantom). Courtesy of G. El Fakhri.

C. Toward reconstruction-free PET imaging

Simon Cherry, from UC Davis, reported about an interesting development on direct positron emission imaging (dPEI) [11]. Using two small BGO crystals with a double-side readout, comprising one very fast micro-channel plate (MCP) and one Silicon photomultiplier (SiPM), and filtering the fastest Cherenkov coincidence events with the help of a conventional neural network, they could achieve a CTR of 40 ps. Similar experiment with lead glass radiation detectors gave 32 ps. They could use this setup to reconstruct the image of a brain phantom using for each event the precise 3D information provided by this superb timing resolution, avoiding therefore the tomographic reconstruction. More details are given in section VII. A. Even if this configuration is certainly not practical for a PET scanner (too small crystals, complex and very expensive readout, very long acquisition time), this is the first demonstration of a reconstruction-free PET image (Fig. 3).

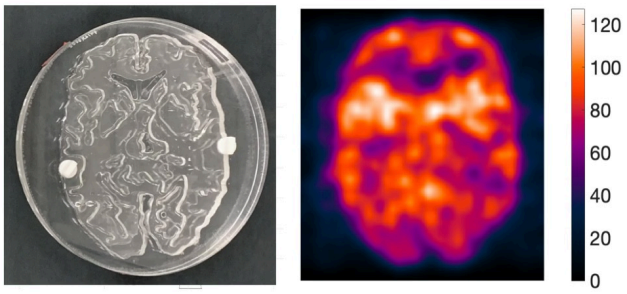

Fig. 3: Reconstruction-free image (right) from a brain phantom (left). Courtesy of S. Cherry. From ref [11].

Simon Cherry pointed the importance of combining the Total Body and the TOFPET approaches for reaching a cost-effective unprecedented SNR, maintaining a high solid angle coverage, while spacing the crystals and reducing therefore the number of channels and associated cost. This would allow routine parametric imaging, ultrafast (1s) imaging, avoiding motion corrections, more precise quantification and kinetic studies.

The strategy in Davis is to exploit the Cherenkov fast luminescence in scintillators with a high refraction index, such as BGO [12] or in dense semi-conductors, where the energy measurement is given by the charge carriers collection and the precise time tag by the Cherenkov emission [13].

D. Brain imaging with TOF

Jae Sung Lee from Seoul National University insisted on the importance of developing dedicated brain PET scanners to face the expected dramatic increase of the prevalence of different forms of dementia in the coming years. In this perspective the necessity to combine high spatial and timing resolution brain imaging devices was highlighted. As the dimensions, and therefore the cost of such an organ-specific PET scanner are limited, this is also a good benchmark to test the different fast timing technologies under development and to validate the clinical impact of good TOFPET performance.

Several projects are proposed in different countries with a target CTR objective ranging from 100 ps to 250 ps. In addition, a good spatial resolution of the order of 1mm is required over the whole field of view, to delineate small cortex structures in particular in the endocortex, where the generation of the tau protein could be detected in the early and non-symptomatic phase of the Alzheimer disease. Such a good spatial resolution for a small ring diameter of about 30 cm requires the determination of the depth of interaction of the γ-rays in the crystals with a precision of a few mm only.

A good timing resolution is important for the image quality, as illustrated in Fig. 4. But in the case of a PET insert in a MRI machine, a combination of high interest for brain studies, improving the PET CTR helps reducing the impact of imprecise attenuation corrections, which is often the case when combining PET and MRI, in contrast to PET/CT.

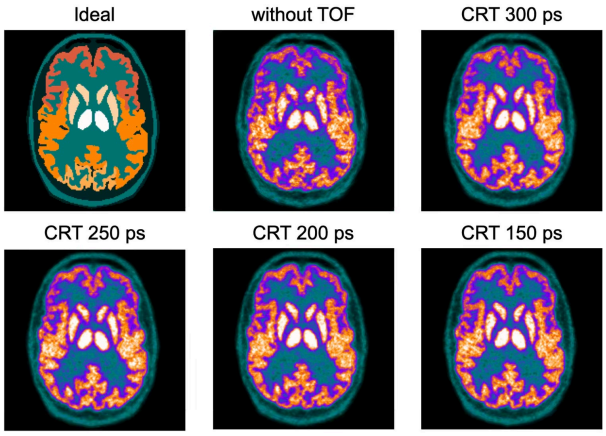

Fig. 4: Simulated brainPET images with different CTR. Courtesy of Jae Sung Lee and Brightonix Imaging Inc.

E. Novel biomarker and drug delivery systems for theranostics – extracellular vesicles

Ewa Stępień from the Jagiellonian University presented the rational of using extracellular vesicles (EV) as a drug delivery system [14]. These nano-/micro-sized cell-derived entities (30 nm–1 μm) have been characterized in experiment from their biologic and chemical point of view (infra-red spectrum, mass spectrometry, mRNA and lipid). These EV can be radiolabeled in different ways (Fig. 5) and serve for theragnostics delivery

of targeted therapy, with the aim of first better understanding their targeting, regulatory function and clearance. In-vivo tracking of EVs in the organism requires good sensitivity and timing performance to assess the biodistribution and pharmacokinetics with good precision.

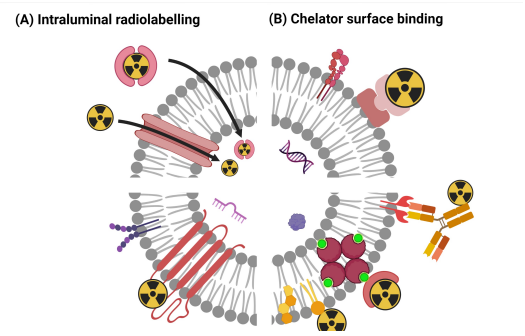

Fig. 5: Extracellular vesicles (EVs) as drug delivery system, with (A) intraluminal radiolabeling, (B) chelator surface binding of free ions, (C) covalent, and (D) ligand surface radiolabeling by organic radiotracers. Courtesy of Dr. E. Stępień, Jagiellonian University, Poland. From [14].

F. The importance of fast-timing gradients in 3T MRI for diffusion and perfusion analysis in Prostate Cancer

Ana Jimenez Pastor from Quibim presented the benefit of fast temporal resolution in prostate magnetic resonance imaging (MRI) using T2-weighted imaging, diffusion weighted imaging (DWI) and dynamic contrast enhanced (DCE) imaging. This allows to quantify the apparent diffusion coefficient (ADC) and vascular permeability (K^{trans}) in multiparametric analysis. With the help of AI techniques, any tissue can thus be characterized into healthy or pathological origin.

Manual segmentation being a time-consuming task, a convolutional neural network (CNN)-based automatic segmentation has been trained to segment the prostate in 3 regions (central/transitional zone, peripheral zone and seminal vesicles). This process was performed in less than 30 s, allowing almost real-time analysis of prostate MRI fast-timing diffusion/perfusion sequences by AI.

III. Concepts and Systems Considerations for High Temporal Resolution in Medical Imaging

This section presents several innovative approaches to improve TOF techniques and take advantage of them. The first sub-section A discusses general considerations about the possibilities offered by progress in several technologies but also the necessity to take-into-account their integration in compact multi thousand channels systems. Sub-sections B to F present different projects integrating TOF features in Total Body PET, BrainPET with metascintillators, small animal and multimodal imaging systems. Finally, sub-sections G to I discusses TOF in the context of positronium studies, hadrontherapy and X-ray CT imaging.

A. Detector design considerations for TOF-PET systems

There is no doubt that the impressive ongoing R&D effort by a growing number of groups worldwide, taking advantage of progress made in a number of emerging technologies, will lead to significant improvements in TOFPET performance, as already explained in [15]. There have been efforts to improve the timing performance of the sub-components of the whole detector chain, such as in the scintillator, photodetector and readout electronics, as shown by N. Kratochwil from CERN (Fig. 6).

However, most of these works still lacks scalability and makes use of bulky electronics that is hardly transferable to industrial devices. Combining them all together in a system, as for instance in a Positron Emission Tomography (PET), is not straightforward, and many considerations are required. Furthermore, a very high level of integration of the current developments must be achieved, in order to be transferred to the industry. The performance of the achieved coincidence time resolution (CTR) for one or few channels has to be integrated in complex multichannel electronics. As discussed at the workshop, the integration of these technologies in complex multichannel systems without compromising the overall performance remains a very important issue that should not be neglected.

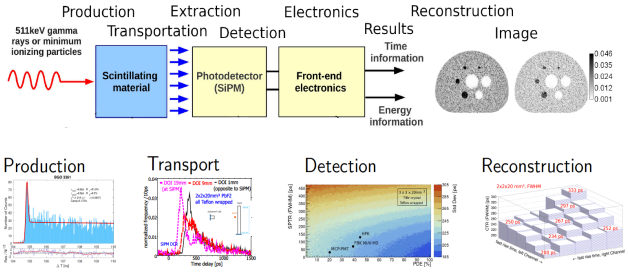

Fig. 6: The timing value chain in a TOF-PET scanner, adapted from [16, 17, 18, 19]. Courtesy of N. Kratochwil, CERN.

Poor detector designs are causing low coincidence detection efficiency, low packing fraction or low detector tile-ability. Concepts of good TOF-PET detector configurations were presented by C. Levin from Stanford University (Fig. 7) and illustrated the importance of 1-to-1 crystal to SiPM coupling for optimizing the TOF resolution. There is also a need for high-precision and scalable readout electronics.

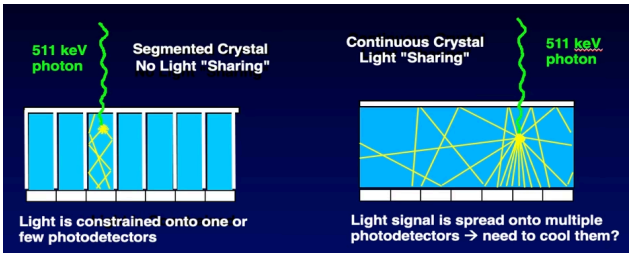

Fig. 7: Better detector SNR can be achieved with 1-to-1 crystal photo-detector coupling, concentrating all the light on a single photo-detector (left). Courtesy of C. Levin, Stanford University, CA, USA.

The use of BGO scintillators is becoming again popular in the last years. BGO was widely used in the past but exhibited some limitations, especially related to timing capabilities. However, when implemented in the form of meta-scintillators with other faster materials, or as bulk material combined with high performance electronics to detect the weak Cherenkov luminescence, it opens a new possibility to reach accurate CTR at moderate cost. Notice that BGO is about 3-4 times cheaper than LYSO.

In this context a work by S. Gundacker and the team in Aachen showed good agreement between simulation and experimental results obtained with high-frequency (HF) electronics for BGO pixels of 3 mm and 20 mm length [20]. The obtained values were 122 ps and 243 ps FWHM, respectively. Currently, they are also combining their tests with the PETsys electronics [20] in order to evaluate the implementation of the HF techniques at a system level.

Another cheap approach is to use pure Cherenkov radiation materials like PbF_2, as suggested by G. Razdevsek, from the Jozef Stefan Institute in Ljubjana. About 10 times cheaper than LYSO, PbF_2 has a very high density of 7.8 g/cc, a Cherenkov threshold at about 100 keV and produces on average 20 Cherenkov photons per 511 keV γ-ray.

B. Design and initial results of a Total Body PET with TOF and Depth of Interaction (DOI) capability

Antonio J. Gonzalez Martinez, lead investigator of the Institute for Instrumentation in Molecular Imaging (I3M) from the Polytechnic University of Valencia presented the initial results for a total-body PET with TOF and depth of interaction (DOI) capabilities. Having in mind a fair compromise between performance and cost, this group is considering a 75 cm axial coverage, a more realistic and economical solution than a 2 m long scanner. Such a machine is entering prototyping foreseen for Autumn 2023.

It is well-known that DOI correction would impact greatly small-diameter systems, but this effect would also impact the long axial field-of-view scanners leading to performance degradation of the lines of response most parallel to the cranio-caudal axis. The I3M technology proposes achieving detectors with both DOI and TOF capabilities. In particular, the design is based on arrays of semi-monolithic LYSO crystals, that have successfully showed to reach an energy resolution of 10±1%, TOF CTR of 221±9 ps and 2.9±0.6 mm FWHM, together with less than 4 mm DOI resolution. When multiplexing readout techniques are used to reduce the cost the energy performance is 13.4%±0.9 and the TOF 305±5 ps CTR. The initial testing of a 10 cm AFOV prototype is underway, even though the delivery of components is suffering unavoidable delays in these post-COVID-19 times.

C. Implementation of a signal reduction scheme for PET with TOF and DOI capabilities

Within the framework of a project to develop a Total-Body PET system, an interesting approach has been developed to reduce the number of channels in a readout scheme, preserving the timing capabilities. Furthermore, the design, presented by a group belonging to I3M in Valencia, enables the capability in the scintillator design to provide accurate depth of interaction (DOI) information. In that work, they have designed a detector block based on arrays of 1x8 slabs of LYSO with 20 mm height and 3 mm size in the pixelated direction (Fig. 8). The array is coupled to a matrix of 8x8 SiPMs and read out by a novel circuitry that reduces the 64 SiPMs signals to 8+8. The reduced signals are read out using the PETsys electronics. The 8 signals along the 8 slabs preserve the timing performance, whereas the 8 signals perpendicular to those allow one to achieve accurate 3D spatial determination, including DOI.

The results show CTR values around 330 ps FWHM for the whole 1x8 crystal array when using this readout scheme, compared to 300 ps FWHM when digitizing all 64 channels. An energy resolution in the range of 12-13% was also achieved. In terms of spatial resolution along the monolithic direction of the slabs and DOI, the system exhibited a FWHM of 2.2 ± 0.5 mm and 3.3 ± 1.1 mm, respectively [21].

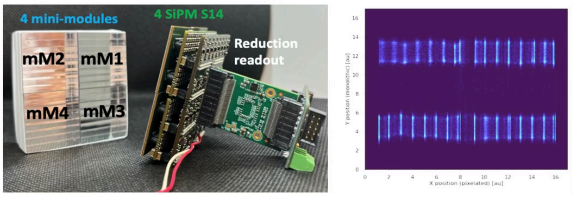

Fig. 8: Left, the 4 arrays of 1x8 slabs and associated electronics. Right, flood map of these 4 blocks. Courtesy of A. Gonzalez-Montoro, I3M (Spain).

D. GATE simulations of meta-scintillators used in a brain dedicated PET

Detectors based on meta-scintillators have been proposed to overcome the timing resolution limits of the commonly used scintillators [22, 23]. These are engineered structures that combine and optimize features of the same heterostructure. These blocks are built for instance alternating thin slabs in the range of 100-300 μm of two scintillation material. A dense material based on LYSO or BGO is combined with a lighter but faster one such as organic scintillators or BaF_2 [23, 24, 25, 26]. More details on scintillators heterostructures are given in section IV. Extensive studies from a simulation and application to a scanner point of view have been made in the frame of a collaboration between Instituto de Pesquisas Energéticas e Nucleares (Brazil), Multiwave Metacrystal (Switzerland) and I3M (Spain).

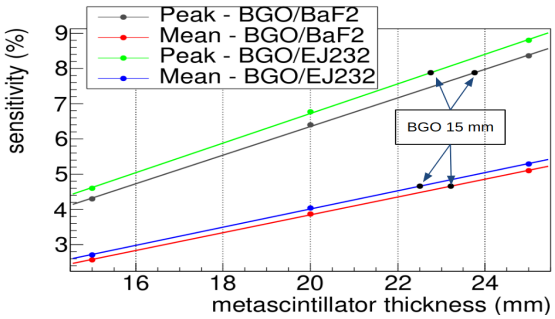

Fig. 9: Simulation plots for the sensitivity (both peak and mean) as a function of the metascintillator thickness. BGO/BaF2 metalayers have 300/300 υm. BGO/plastic EJ232 have 300/100 υm. Sensitivity for bulk BGO with 15 mm thickness is indicated as a reference. Courtesy of D. Bonifacio, Instituto de Pesquisas Energéticas e Nucleares (Brazil), Multiwave Metacrystal (Switzerland) and I3M (Spain).

Simulations of different meta-scintillators have been carried out, following a brain dedicated PET geometry. In particular, in that work BGO/BaF_2 and BGO/plastic were tested. The results have also been compared to designs based on bulk materials (LYSO and BGO). The PET geometry has 290 mm in diameter and 175 mm axial length. From these investigations, an equivalent length of 23.7 – 23.8 mm of both BGO/BaF_2 and BGO/plastic was required to obtain the same peak sensitivity as bulk 15 mm height BGO or 20mm height LYSO (Fig. 9).

E. Time of flight progress in small animal research

The application of precise CTR to small animal imaging is complex because the aforementioned benefits are hardly observed unless reaching very accurate timing performance [27]. In this context, researchers at the I3M in Valencia are working on a PET implementation based on two rings of detectors, namely a scatter and an absorber (Fig. 10). Events that undergo a first interaction in the scatter and get stopped in the second allow to improve image reconstruction quality by using cones of response instead of conventional lines. However, these techniques require precise timing information of the two interactions. In that work, an inner ring based on LYSO:Ce,Ca co-doped crystals arrays of 1x1x3 mm^3 has been designed. 24x24 crystal pixels are coupled to 8x8 SiPMs with 3x3 mm^2 active area (type S13361-3050 from Hamamatsu Photonics). That means that groups of 9 crystals are coupled to a single SiPM. This approach allows to reach high timing and spatial capabilities with a reduced number of channels. The TOFPET2 readout from PETsys electronics has been used [28].

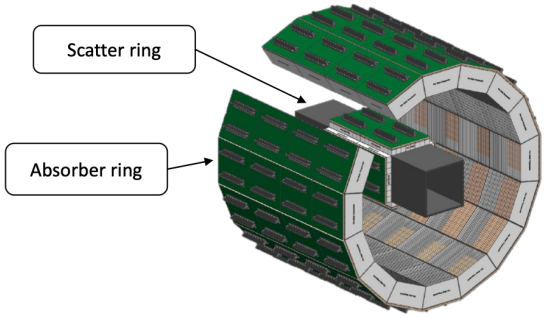

Fig. 10: Sketch of the two ring systems: Compton-PET approach. Courtesy of C. Valladares, I3M (Spain).

In terms of results, an average CTR of individual pixels of 165 ps FWHM was observed for an energy range of 450 – 600 keV. This slightly deteriorates to about 300 ps for the scatter energy range of 230 – 450 keV. All pixels are well resolved, as it can be observed in the preliminary flood map in Fig. 11 left. Another interesting observation in this work refers to the transit time spread in the SiPM. For a given SiPM we can observe a variation in the CTR centroid of up to 40-50 ps [28]. It would be mandatory to take this into account when the image reconstruction considers multiple pixels and TOF.

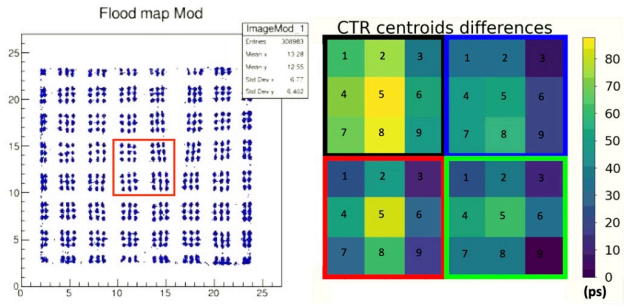

Fig. 11: Left, flood map of the 24x24 crystal pixels. Right, SiPM time spread for the central 4 SiPMs. Courtesy of C. Valladares, I3M (Spain).

F. TOF PET in multimodal imaging systems

1) Description of a 100-ps CTR TOF-PET for PET/CT neuroimaging

This project addresses the need to increase light collection and decrease sources of temporal variation in scintillations detectors by influencing the light collection efficiency to photodetector per interaction, photon interaction depth with respect to the photodetector, the scintillation light transport transit time to photodetector and the readout electronic noise. This is achieved with a novel crystal to photosensor coupling configuration using side readout instead of end readout [29, 30]. Such fast LGSO experimental setup achieved an average CTR of 103.3±0.7 ps [cf. above]. Such a prototype would require 16 modules (full-ring = 64 modules with a power consumption of about 670 W)

2) Description of a 2nd-generation 230-ps CTR TOF-PET for PET/MR neuroimaging

The advantages of combining two strong clinical information-carrying modalities, such as PET and MRI are obvious and can offer the best of both worlds to characterize tissue and biology. Furthermore, a PET insert would allow any existing MR system to be used without room renovation at a 5–10-fold lower costs than an integrated PET/MR system. However, many challenges remain in setup time, registration of PET and MR datasets, as well as radiation safety in the MR center (although this might be less of a problem if high-sensitivity is achieved below the radioactivity exemption limit (e.g., 70 MBq for ^{18}F-FDG in Switzerland). The presented 2nd-generation RF-penetrable insert developed in C. Levin's lab allowed 230 ps CTR TOF PET imaging with stable PET performances (CTR, energy resolution, single/coincidence count rate) independently of the MR field and sequences, and excellent MR image quality with running PET detectors [29].

G. On a way to clinical positronium imaging with the high time resolution total-body J-PET system

Pawel Moskal from Jagiellonian University in Poland presented on behalf of the J-PET collaboration their multiphoton and positronium imaging system (e.g., for radionuclides such as ^{68}Ga, ^{44}Sc) [32, 33] using plastic scintillator detectors to develop cost-effective total-body PET.

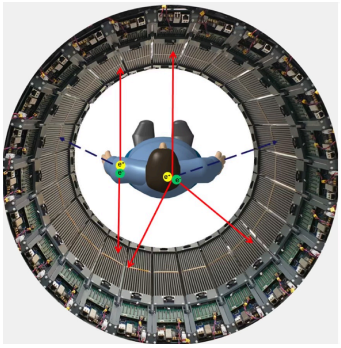

Fig. 12: Clinical positronium imaging prototype with high time resolution in a whole-body setting. Courtesy of P. Moskal, Jagiellonian University, Poland.

They also presented the very first in vivo positronium imaging images showing the proof of principle of the J-PET system with convincing evidence and promising results. Fig. 12 shows the J-PET prototype with 50 cm axial field-of-view, consisting of 24 independent modules each built from 13 plastic scintillators strips. The modular PET, with axially arranged plastic scintillators, is constructed as a prototype of cost-effective total-body PET systems [31, 32]. The superimposed arrows indicate annihilation photons (solid arrows) and prompt photons (dashed arrows). The possibility of multi-photon registration (2-annihilation plus prompt) or (3-annihilation + prompt) opens perspectives for positronium lifetime imaging and for multi-isotope imaging [33].

H. Development of a fast Cherenkov detector dedicated to prompt gamma time imaging

Maxime Jacquet from the TIARA collaboration (Time-of-flight Imaging ARrAy) in Grenoble presented the conception of a clinical application of prompt-gamma detection for online monitoring of hadrontherapy.

They used a diamond-based beam monitor and 30 PbF_2 1×1×1 cm^3 crystals with SiPM readout and performed Monte-Carlo simulations for a reconstruction algorithm based on prompt-gamma time measurement for 63 MeV protons [33].

They created a high-sensitivity (~1%) prompt-gamma detector with a 4 mm proton range determination using only 600 prompt-gamma rays and a 256 ps CTR. This allowed to go towards the next generation of detector design (Fig. 13).

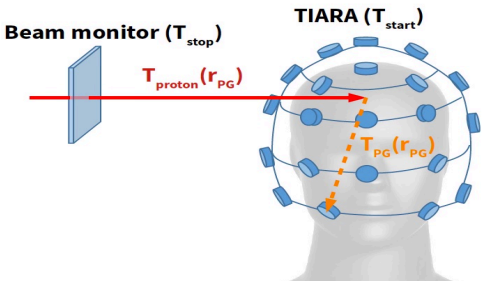

Fig. 13: Prompt-gamma time imaging showing the beam monitor and the 30 elements PbF_2 crystal array. Courtesy of M. Jacquet, TIARA Collaboration, Grenoble, France.

I. Toward a First Prototype Time-of-flight CT Scanner

Julien Rossignol from the Université de Sherbrooke in Canada presented their project of TOF CT prototype (Fig. 14). In X-ray CT imaging, timing can bring information on scattering which is affecting image quality by degrading contrast-to-noise ratio (CNR) and producing the so-called "cup and streak artifacts). GATE simulations have proved the interest for real-time discrimination of individual photon timing using fast detectors, TOF and ultra-short pulsed X-ray source [34, 35]. A total timing (source + detector) of 10 ps would be required for optimal performance

TOF-CT brings about significant CNR improvement (+20%) and dose reduction that still need to be implemented in practice. As no commercial pulsed X-ray source with energy >40 keV existed, the authors developed and tested a X ray prototype source. The detector electronics was also aiming at 200 ps TOF with a 64×4mm^2 detection area with a 16 channels data acquisition system. For the next generation system with full fan-beam detector, data compression would be desirable, as data generation could reach up to 120 TB/s for a 14×14 in^2 detector, which can be addressed using Edge machine learning.

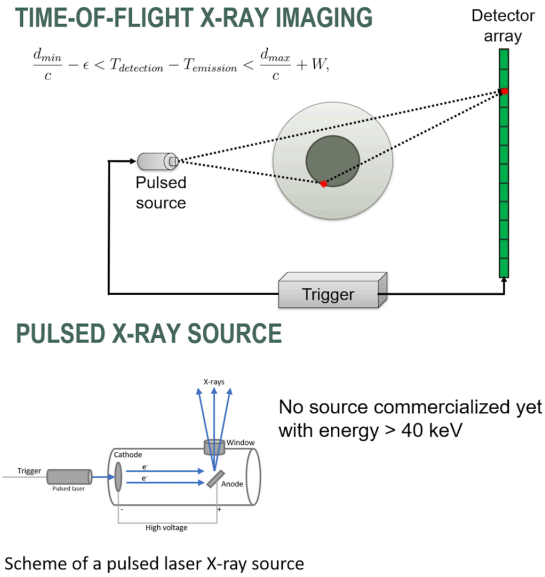

Fig. 14: TOF X-ray imaging principle (*top*) and pulsed laser X-ray source prototype (*bottom*). 10ps TOF performance would allow rejecting scattered X-rays and improving the image contrast. Courtesy of J. Rossignol, University of Sherbrooke.

IV. Advancing Scintillator Technology for Enhanced TOF Performance

This section is divided in three sub-sections. The first one A focuses on the identification of the parameters influencing the timing performance of scintillators, on recent advances for improving their timing properties as well as on the techniques for the detailed investigation of the timing sequence of the complex energy relaxation schemes leading to the scintillation process. Sub-section B concentrates on the new concept of scintillation heterostructures allowing the production of a bunch

of additional prompt photons on top of the scintillation pulse from a standard scintillator. Sub-section C introduces the concept of metascintillators, where nanoscintillators and a number of nanophotonics features can further boost the performance of such heterostructures much beyond the state-of-the-art.

A. Engineering scintillators for fast timing applications

In the quest for fast timing scintillation, several approaches have been investigated over the last decade to increase the fraction of fast timing processes in "standard" scintillators by engineering the band structure of the materials.

1) Main parameters influencing the scintillator time performance

The scintillation mechanism in a scintillator is a complex process starting from the creation of hot electron-hole pairs to the generation of the scintillation light [36] and results in intrinsic limit of the timing performance of standard materials. The scintillation light is generally described by a bi-exponential expression:

$$I(t) = \sum_j \frac{f_j}{(\tau_{dj} - \tau_{rj})} \left[e^{-(t-t_0)/\tau_{dj}} - e^{-(t-t_0)/\tau_{rj}} \right]$$

characterized by the light produced I(t), the rise (τ_r) and decay time (τ_d) for different scintillation centres j with a fraction f_j [19]. Timing can be expressed as the ratio of the light yield of the scintillator by the product of emission rise and decay time. The timing resolution of a scintillator is in first approximation proportional to the square root of inverse photon density N_{ph} [37]:

$$time\ resolution\ \alpha \sqrt{\frac{\tau_r \tau_d}{N_{\mathrm{Ph}}}}$$

Therefore, recent scintillator developments aim at achieving a maximum light yield with the shortest possible rise and decay times to minimise timing resolution either by modifying scintillation properties of existing materials or by an improved exploitation of their prompt photon emission.

2) Acceleration of the light emission in standard scintillators

One way to improve the timing resolution of known standard scintillators (both intrinsic and activated materials), which have been largely investigated over the last years, is to reduce the delay between the creation of the hot electron-hole pairs and the capture of the resulting slow charge carriers by the luminescent centres after their multiplication and relaxation in the medium. Alternatively, it is possible to favour a direct exciton relaxation or trapping by the luminescent centres. This has been successfully achieved in intrinsic scintillator such as $PbWO_4$ with a high-level doping of trivalent cations such as La^{3+} or Y^{3+} [38, 39, 40, 41], or in cerium activated scintillators such as orthosilicate (LSO/LYSO) [42, 43, 44] and in garnets (YAG, LuAG, GAGG) [45, 46, 47, 48, 49], co-doping them with divalent cations such as Ca^{2+} or Mg^{2+}. The introduction of a divalent cation favours the creation of Ce^{4+} which, in the process of the capture of electrons from the bottom of the conduction band at the latest stage of the scintillation process, strongly competes with traps and opens an additional route for the electron hole radiative recombination in cerium ions, resulting in a faster light emission. An example of such an acceleration of the decay time components with the increase of co-dopant concentration is illustrated in Fig. 15, showing recent results obtained on a set of GAGG samples with increased of both cerium and magnesium doping concentrations [50]. A decrease of the decay emission response by more than a factor of ten is observed due to the increase of the dopant concentration. However, this strong reduction of the decay time had no impact on the timing resolution because it resulted from a quenching of emission and therefore a reduction of the light output [50].

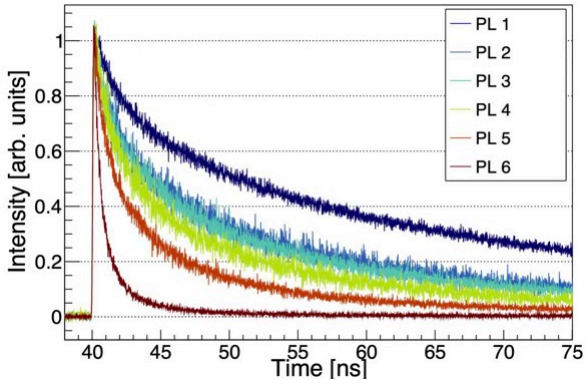

Fig. 15: Decay emission spectra for a set of GAGG samples with increase of Ce, Mg concentration with increasing concentration from PL1 to PL6. Courtesy of E. Auffray, CERN. Figure modified from ref [50].

To guide experimentalists to the "design" of the band gap and defect engineering aiming at favoring fast recombination and capture of electrons and holes at the emission luminescent centre, detailed numerical modelling approaches of band structure and defect calculation are useful. Several developments in this domain, using in particular the density function theory (DFT) are more and more exploited [51, 52, 53]. Combining experimental and theoretical approaches is the route toward progresses in the direction of a better understanding and an optimized engineering of scintillators for fast timing.

3) Better exploitation of Cross-Luminescence

Cross-luminescent materials are known since many decades for exhibiting a very fast sub ns emission. This emission is due to a radiative recombination of electrons from the valence band with the holes in the uppermost core band when the non-radiative Auger recombination process is not possible, because of an energy gap between the forbidden band larger than the energy between the valence band and core band [54,55]. This is the case for BaF_2, one of the most popular cross-luminescent

material. The large quantity of delocalized electrons in the valence band allows their very fast recombination with the holes in the core band. However, the cross-luminescence emission has not been extensively exploited due to two main drawback properties: The fast cross-luminescence (600 ps decay time for BaF_2) occurs generally in the deep UV (200 nm) wavelength region, for which the photodetection efficiency of most photodetectors is low, and in many cases this very fast emission is accompanied by a self-trapped exciton emission characterised by a much slower emission (600 ns for BaF_2). In the last years two approaches have been investigated to improve the potential of cross luminescence materials to be used in fast timing detectors:

- Suppress the slow component to keep only the fast emission,
- Develop cross luminescent materials with emission in a higher wavelength range.

Regarding the first approach, the doping of the material is an appropriate solution to reduce the slow component and has been successfully applied by several groups to BaF_2 crystals [55, 56, 57, 58]. An illustration of this is presented in Fig. 16, showing the decay spectra of undoped and Y doped BaF_2 at different Y concentrations produced by SICCAS in Shanghai. A strong suppression of the slow component is observed with the increase of Y concentration without affecting the very fast cross-luminescence emission [58] with the consequence of reducing the light output. This feature would allow to reduce the pile up effect while keeping the very good timing resolution and therefore making BaF_2 an interesting time tagger for applications with fast event rates, for instance as a component of scintillator heterostructures. as described in section IV-B.

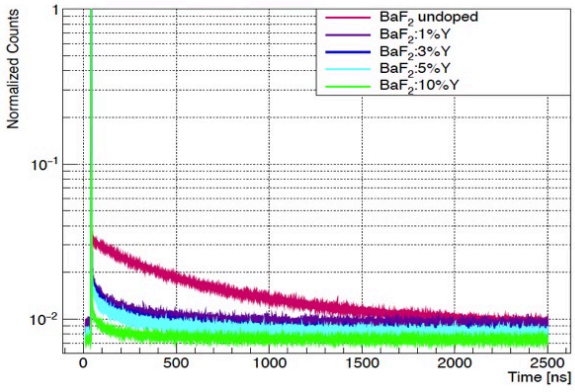

Fig. 16: decay spectra of BaF_2 crystals from SICCAS with different concentrations of Y. Courtesy of R. Cala, E. Auffray, CERN Crystal Clear team

The second approach of material research with long wavelength cross-luminescence emission has been pursued by several groups and in particular by the group of the University of Tartu in Estonia and the Czech Academy of Science in Prague, Czech Republic [59, 60]. Materials with shifted emission wavelength to the red have been produced.

Due to their complex valence and core band structure, the family of ternary halides of alkali and alkaline-earth metals are considered as to be particularly promising candidates [52, 59, 60] an example of decay time spectra obtained on $CsCaCl_3$ is presented in figure 17 [60].

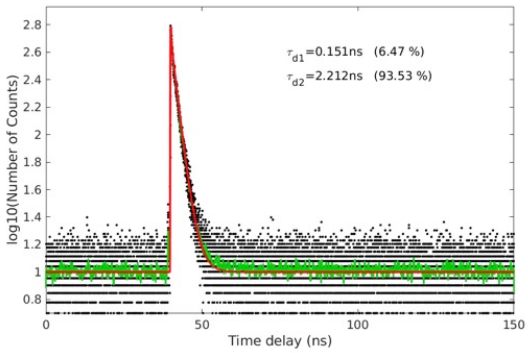

Fig. 17: Decay spectra of $CsCaCl_3$ crystal produced by FZU, Prague, Czech Republic. Picture modified from Ref [60]

4) Towards a 1-ps CTR TOF PET

An ultimate approach for improving the time resolution is to exploit sub-ps transient phenomena taking place when ionization radiation interacts with a medium. In transparent scintillators the polarization of the environment near the particle trajectory produces of hot polaronic states, which locally modify the refractive index and polarization of the medium [61]. An intermediate goal towards this 1 ps target, which cannot presently be achieved with scintillating detectors is to develop faster alternatives to probe these transient phenomena with high frequency external signal, following the principle of a heterodyne detection. Only such a paradigm-change of detecting optical modulation of a laser probe by ionizing radiation would allow to go faster than scintillation with a femtosecond temporal resolution, as proposed by C. Levin and his group, from Stanford University [62]. This novel approach would require novel detector configuration to achieve high sensitivity to small optical modulations.

5) Characterization methods

A deeper understanding of the scintillation mechanisms allowing to exploit or to improve fast emission processes cannot be achieved without the development of more advanced characterization methods which are nowadays possible thanks to the availability of fast and high-performance instrumentation.

Among the various methods the transient optical absorption techniques is a tool allowing to study the dynamics of the population of energy states involved in the late-stage carrier relaxation process and therefore to understand the role of some energy states in the scintillation process. This procedure is based on the pump and probe method: using a tunable-wavelength femtosecond laser as pump to excite specific energy states and to monitor the de-excitation kinetics by measuring the transient absorption at different times after excitation with a broad band laser pulse.

This technique has been extensively used over the last years by Vilnius University [63, 64, 65, 66].and has shown to be extremely powerful for deciphering all the transient phenomena leading to the scintillation, a key for better understanding and exploiting them for the development of a new generation of fast scintillators.

B. New approaches for improving TOFPET performance: scintillator heterostructures

The idea of boosting the number of prompt photons available for 511keV gamma-time-tagging is one of the pillars of the 10 ps TOF-PET challenge. Looking at the landscape of fast luminescence phenomena, emerging materials featuring a high photon-emission rate can be integrated within current radiation detector technology by sampling the scintillator pixel geometry. Such proof-of-concept layered design based on a dense state-of-the- art scintillator and a fast photon-emitter was previously demonstrated in a small 3x3x3 mm^3 pixel geometry [23] using both plastic scintillators and nanocrystals as the source of prompt photons.

A dedicated session of the workshop focused on the advances of this new detector concept using heterostructure scintillator pixels with sizes relevant for the efficient stopping of 511keV gammas. The results presented showcase the complexity and potential of the technique in pixels up to 15-20 mm long, together with the improvements and limits in terms of overall stopping power, energy- and time-resolution performances. In addition, first time results on the depth-of-interaction encoding offered by such scintillator heterostructure concept has been demonstrated and this is being considered as a new added functionality in a scalable detector geometry.

1) Energy sharing concept

The mechanism allowing to incorporate prompt photons into the gamma detecting signal relies on the range of the recoil photoelectron in the given high-Z material, i.e. around 400 µm for LYSO:Ce and BGO. Therefore, sampling the scintillator pixel with a pitch between 100-200 µm allows to have a significant percentage of events where the energy from a photoelectric effect is shared between the 'slow' and the 'fast' material as shown in Fig 18.

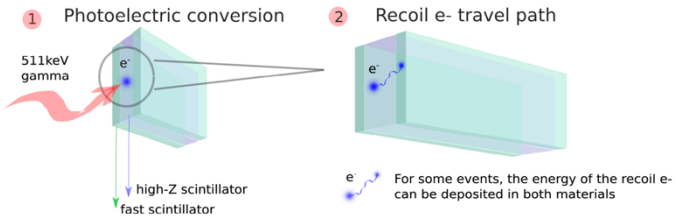

Fig 18: Energy sharing concept for 511 keV gamma detection using a pixel heterostructure design featuring two scintillators, a dense high-Z material for the stopping power and fast photon emitter dedicated to timing. Courtesy of R.M. Turtos. Aarhus University. As published in [23].

This concept presents clear advantages for improving time resolution. However, it imposes some challenges for the overall energy resolution of the pixel, especially when light output matching is not achieved. The following sections highlight the results obtained using heterostructure scintillator pixels based on BGO, a first step in the direction of metascintillators, where the fast scintillator will include ultrafast nanoscintillators and photonic features will be included for a better management of the light transport to the photodetector.

2) Inorganic-organic heterostructures

The luminescence mechanism in organic scintillators happens through relaxation of molecular excitation and is characterized by fast decay times on the order of few nanoseconds. For the metapixel tests, the plastic scintillator EJ-232 from Eljen technology was chosen due to its fast rise and decay times of around 30 ps and 1.6 ns respectively [67]. These values combined with a light output of 8000 ph/MeV yields a photon emission rate of 5 ph/MeV/ps, which is a factor 5 larger than LYSO:Ce and more than 150 times compared to BGO, disregarding Cherenkov emission.

Several combinations have been explored by different groups, using BGO and EJ-232 plates with thickness between 100 and 200 µm. Pixels were assembled by Crystal Photonics Inc. or at CERN workshop using long-faces polished plates. The timing performance has been evaluated following the method reported here [23, 24, 26], using time-of-flight coincidences and metapixels coupled to UV sensitives SiPMs combined with fast high-frequency readout electronics [66, 67]. Event identification is based on the 2D distribution of the integrated-charge as a function of the pulse's amplitude, from which several other methods can be followed, i.e. change of coordinates to energy deposition, rise time distribution estimator, etc. An example of the 2D event map in terms of the energy deposited in both material for a BGO/EJ232 3x3x15 mm^3 heterostructure pixel is shown in Fig. 19.

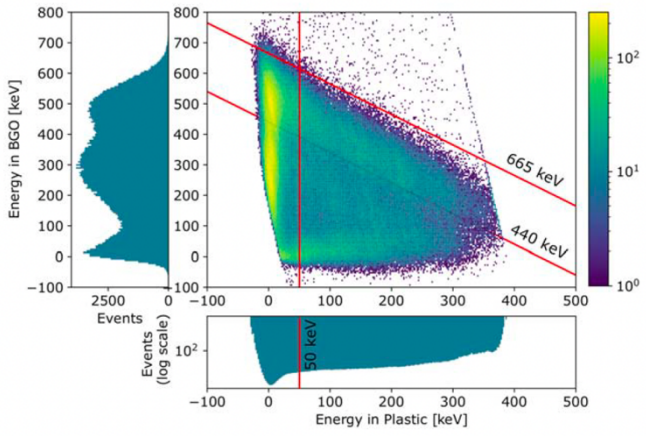

Fig 19: 2D histogram of 511keV gamma energy deposited in BGO/EJ232 3x3x15mm^3 heterostructure scintillator following a change of coordinates from amplitude and integrated charge to energy deposition, as published in [26]. Courtesy of F. Pagano, CERN.

CTR values of around 200 ps were obtained for all events depositing 511keV in the 3x3x15mm^3 BGO/EJ232 heterostructure pixel using 200 µm thick plastic plates. A slight improvement down to 173 ± 9 ps is observed for shared events with more than 50 keV deposited in the plastic material [26]. These results are consistent among the different research groups

leading this topic (Multiwave Metacrystal SA, I3M Valencia and CERN). Despite the complexity of the technique in terms of the pixel fabrication, the excellent timing performance of LYSO:Ce crystals is now within reach using two low-cost and well established scintillator materials.

3) *Cross-luminescent heterostructures*

Another interesting idea makes use of the fast emission generated from the radiative recombination between valence electrons and core holes known as cross-luminescence. As mentioned in section V, this emission seats in the deep UV region of the electromagnetic spectra, features sub-nanosecond decay times and can be found in materials such as BaF_2. Metascintillator pixels composed of BGO and BaF_2 exhibit a higher effective density compared to plastic-based compositions and this increases the efficiency of 511keV gamma detection.

However, the cross-luminescence emission in the 200-250 nm range imposes some challenges on the photodetection side [58] and some developments in the detector chain has been implemented. The timing amplification stage inspired by Stefan Gundacker, following Joshua Cates work and their high-frequency readout [68, 69] has been modified by Riccardo Latella from Multiwave Metacrystal SA., following the schematics in Fig 20, together with the use of VUV-SiPMs from FBK. A shift towards lower values in the rise time distributions (RTD) for all detected events can be observed in Fig 21 when comparing NUV and VUV-based technology coupled to BGO scintillators. This points towards a more efficient harvest of Cherenkov or cross-luminescence photons using VUV SiPMs.

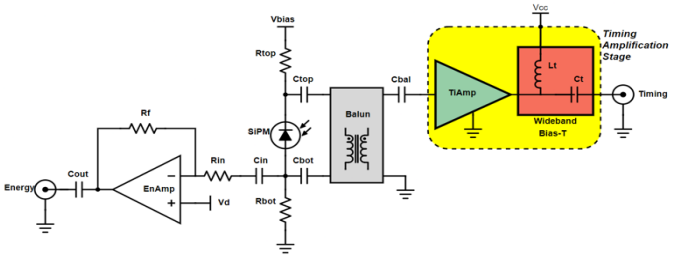

Fig 20: Energy and timing amplification SiPM readout used for the determination of coincidence time resolution of scintillator metapixels at the I3M and Multiwave, Valencia. The circuit is a modification of the one proposed in [68, 69]. Courtesy of Ricardo Latella, Multiwave Metacrystal SA.

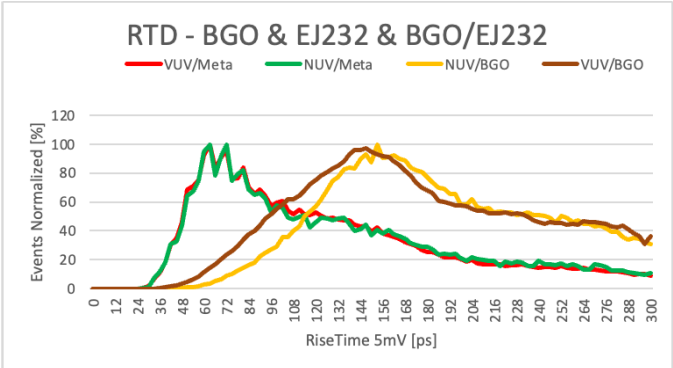

Fig 21: Rise time distribution (RTD) for all 511 keV detected events in a BGO/EJ232 metapixel using NUV and VUV SiPMs from FBK. Courtesy of Georgios Konstantinou and Ricardo Latella, Multiwave Metacrystal SA.

The developments described above, yielded CTR values for a 3x3x15 mm^3 BGO/BaF_2 metapixel of 242 ps for all 511 keV gamma events [25]. Such timing performance was presented to be under improvement by looking into the signal rise time at around 5mV from the baseline during event identification. The preliminary results obtained showcase the potential of this scintillator heterostructure approach based on cross-luminescent materials and BGO for outperforming LYSO:Ce.

4) *Depth-of-interaction encoding*

Understanding light transport in such long heterostructures is of upmost importance for timing optimization and the validation of Monte-Carlo based simulation in use for future detector design. In this regard, the work from the CERN group proves that such heterostructure concept using BGO and EJ232 slabs hold potential for encoding the gamma depth of interaction (DOI) information [26]. In the study, they show the dependence of the CTR performance of short and long crystals with the shift of the coincidences peaks as a function of five DOIs layers within the pixel. This fine correlation enables the estimation of the CTR performance in long crystals by a simple correction that considers the time of the gamma travel path for the different DOI layers as shown in Fig. 22.

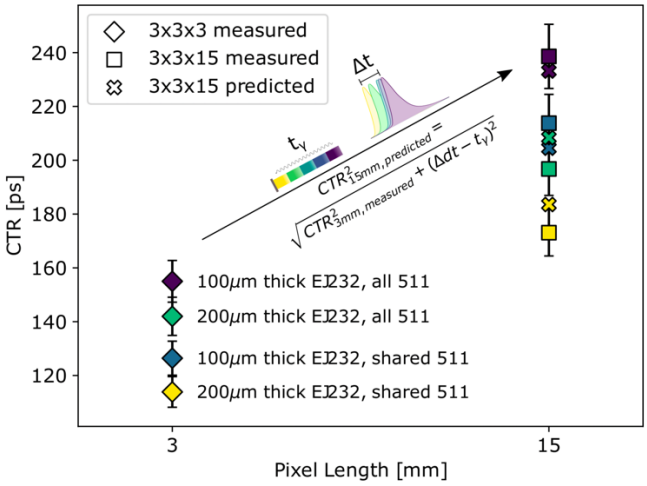

Fig 22: Correlation between the CTR obtained with 3 and 15 mm long BGO/EJ232 heterostructures as a function of DOI as published in [26]. Courtesy of F. Pagano, CERN.

The scaling of the scintillator metapixel concept into large detector modules fits well with the semi-monolithic approach used at Multiwave Metacrystal SA. and I3M [21], where a pixelated design is kept in only one dimension for the optimization of both DOI encoding and timing. Such performance for a 50x50x12-16 cm^3 detector design based on semi-monolithic heterostructures as depicted in Fig 23. is currently under investigation using GATE for the gamma and optical tracking and a neural network for the positioning and timing of 511 keV events.

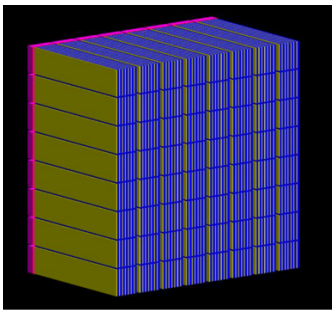

Fig 23: Schematics of the semi-monolithic heterostructure detector approach under investigation. Courtesy of Lei Zhang, Multiwave Metacrystal SA.

C. New approaches for improving TOFPET performance: Nanoscintillators and Nanophotonics

If the potential of scintillator heterostructures has been demonstrated, when combining the high stopping power of standard scintillators like LYSO or BGO with fast organic (EJ232) or cross-luminescent (BaF2) scintillators, their performance is still limited by the light yield and decay time of plastic and cross-luminescent scintillators. The request to break the 100 ps barrier for the coincidence time resolution and to eventually reach the 10 ps target proposed by the 10 ps TOFPET challenge imposes developing the concept of metascintillators with embedded quantum optics and nanophotonic features. A dedicated session of the workshop focused on the huge potential and problematic of introducing such features in a new generation of ultrafast, stable and cost-effective scintillators.

1) Theory of nanoscintillators

Nanoscintillators are known for their high quantum efficiency and fast scintillation properties. A large effort has been made in the recent years to better understand the mechanisms of their interaction with ionizing radiation and the behavior of the resulting excitons in quantum confined systems [70, 71]. Much progress has also been made in the development of cost-effective production methods of semi-conductor nanoscintillators of different composition, with so-called wet colloidal technologies, opening the way to engineering their properties.

When an exciton is confined in a volume smaller than its natural extension in free space (its Bohr radius) its energy levels are discretized with a gap increasing with the confinement strength. As a result, the emission wavelength is directly related to the nanocrystal size and can be tuned accordingly. Moreover, there is no broadening of the energy levels, leading to quasi-monochromatic emission lines and the eh recombination rate is increased, resulting in faster scintillation kinetic than in bulk material. The scintillation decay time can reach sub-ns values if multi-excitons are produced in the same nanostructure, increasing the eh pairs recombination rate probability and therefore decreasing the decay time like the square of the number of excitons (Fig. 24). increased, resulting in faster scintillation kinetic than in bulk material. The scintillation decay time can reach sub-ns values if multi-excitons are produced in the same nanostructure, increasing the eh pairs recombination rate probability and therefore decreasing the decay time like the square of the number of excitons (Fig. 24).

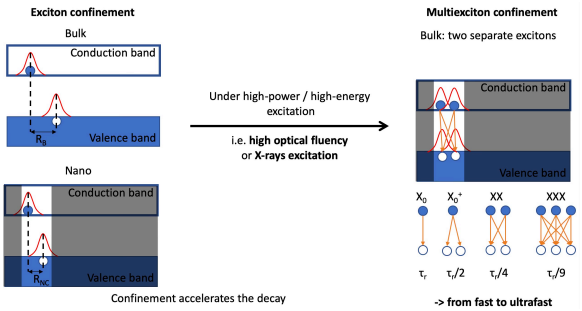

Fig.24: Exciton radiation relaxation from bulk (top left) to single-confined exciton (bottom left) and to multiple-confined excitons (right). Courtesy of B. Mahler, ILM Lyon.

This is for instance the case in CdSe nanoplatelets under X-ray or γ-ray excitation, benefiting from the non-uniform Landau distribution of dE/dx energy deposition of photoelectric and Compton recoil electrons, resulting in small blobs (few tens of nm) with very high ionization density.

Most of the nanoscintillators are suffering from strong self-absorption due to a small Stokes shift, with an important overlap of the scintillation spectrum with the onset of the absorption spectrum. However, in some cases, Coulomb interactions in the multi-exciton regime red-shifts the emission spectrum and reduces the self-absorption, as for CdSe nanoplatelets, with a large 35 meV bi-exciton binding energy and a recombination lifetime as short as 144ps (Fig. 25) [72].

Much progress has recently been made on the synthesis of 2D CdSe nanocrystals [73, 74].

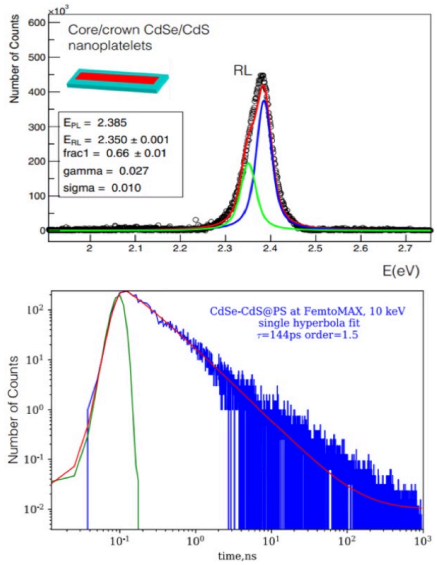

Fig. 25: Radioluminescence RL (top) and decay time (bottom) spectra of CdSe/CdS nanoplatelets. The RL spectrum shows the contribution of a red-shifted bi-exciton component (green curve) on top of the single exciton emission line (blue curve). Courtesy of A Mislovska and I. Moreels, Ghent University, adapted from Ref [72].

The theoretical quantum yield of quantum confined exciton radiative recombination is generally very high, approaching unity, in strong contrast with bulk scintillators, where it barely reaches a few percent. However, the unfavorable surface-to-

volume ratio of nanocrystals opens a number of non-radiative Auger or surface defect induced recombination channels, which compete with the radiate ones. If this has the positive consequence of further decreasing the scintillation decay time, it reduces the scintillation yield. A good way to alleviate this problem is to passivate the nanocrystal surface by engineering core-shell structures, such as CdSe/CdS crown-shell nanoplatelets, offering a good compromise between scintillation kinetics and quantum yield [72].

2) Perovskite nanocrystals

Among a large variety of nanoscintillators potentially interesting for fast timing applications, such as CdSe, ZnO:Ga, HfO_2, halide perovskites deserve a particular attention because of their unique properties [75]. On one side, halide perovskites are direct band gap semiconductors, characterized by an exceptionally high density of states in the lower part of the conduction band, mainly populated by Pb p electronic states, several orders of magnitude stronger than that in Si. As a result, they have a strong interband transition dipole moment, yielding a high absorption coefficient and high quantum yield for the emission of light. They also benefit from a high tolerance to defects for luminescence, good exciton stability at room temperature and low production cost, which make them candidates of choice for photovoltaic, LED and laser applications.

Mixed organic-inorganic perovskites also offer interesting perspectives in terms of luminescence properties and surface passivation, compensating for instance bromide vacancies in $CsPbBr_3$ with methylammonium, boosting their quantum yield, radiation hardness and high temperature stability [76].

An attempt has been made to directly deposit layers of $CsPbBr_3$ nanocrystals on GAGG:Ce plates with two different spin-coating methods [77]. The idea was to evaluate the potential of perovskite nanocrystals as generators of prompt photons in scintillator heterostructures. The so-called static and dynamic spin-coating methods related to the rotation stopped (static) or maintained (dynamic) during the nanocrystal solution drop deposition on the GAGG plate. The static method produced better film homogeneity, which reflected in slightly better radioluminescence intensity. An interesting synergetic effect is observed, resulting in an enhanced radioluminescence intensity of the nanocomposite as compared to bulk GAGG with 2 ultrafast scintillation components of about 100 ps and 700 ps (Fig. 26).

3) Nanocrystals embedded in polystyrene

In order to ease the integration of nanocrystals in metascintillators, while preserving a reasonable light transport efficiency of the prompt photons to the photodetector intensive R&D efforts are ongoing for embedding these nanocrystals in transparent polystyrene films. Not only the high density of semiconductor nanocrystal will contribute to increase the detection efficiency of standard plastic scintillators and consequently of the whole scintillator heterostructure but interesting excitation transfer mechanisms between the nanocrystal and the host polystyrene can be exploited, such as Förster resonance dipole-dipole energy transfer or more generally in a metal-organic framework (MOF) scheme [78].

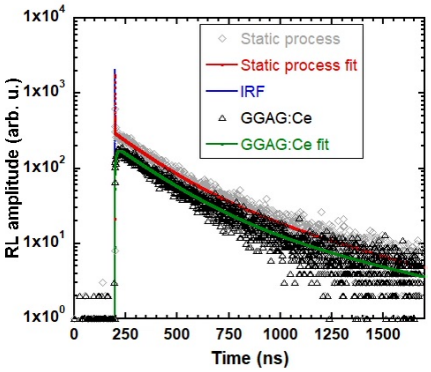

Fig. 26. Scintillation decays in the long time window of CsPbBr3 film on GGAG:Ce prepared by the static method (grey diamonds, red line) compared to the scintillation decay of the pure GGAG:Ce (black triangles, green line). Blue line represents the instrumental response function (IRF). Courtesy of E. Mihokova, Institute of Physics, CsAS. From [77].

$CsPbBr_3$ perovskite and ZnO:Ga nanocrystals have been selected for their very fast scintillation kinetic properties (with decay time components ranging from 40 ps to 350 ps) and different approaches to integrate them in polystyrene host films have been investigated. For ZnO:Ga a hot pressing method has been used, mixing ZnO:Ga powder with polystyrene pellets and hot pressing the compound at a temperature between 100 and 200°C [79]. Transparent films could be obtained with a loading factor of up to 10% weight (Fig. 27 left).

For CsPbBr3 a different method has been used. The polystyrene pellets have been first dissolved in toluene before adding $CsPbBr_3$ nanocrystals in the solution [80]. The toluene has been then slowly evaporated at room temperature. Transparent films with 1%, 5% and 10% weight loading have been obtained (Fig. 27 right).

Work is going on to improve the preparation techniques and increase the loading factor, but first tests in combination with LYSO plates show promising results, particularly for the perovskite samples, with an improvement by a factor 2 of the LYSO timing resolution.

Fig. 27: Left: 10% weight ZnO:Ga nanocrystal loaded polystyrene film from [80]. Right: 1%, 5% and 10% weight $CsPbBr_3$ nanocrystal loaded polystyrene film from [80]. Courtesy of K. Decka, and L. Prouzova Prochazkova, Czech Technical University of Prague.

4) GaN-InGaN multiple quantum wells

Another possibility to produce prompt photons in nanostructured systems is to confine electrons and holes in multiple quantum wells GaN/InGaN heterostructures, where they can radiatively recombine with a very high quantum efficiency. As shown in Fig. 28, one advantage of such structures is to separate the regions of eh pair creation to the

smaller bandgap regions of their recombination, which is therefore red-shifted as compared to the excitation energy. The self-absorption can be therefore reduced as compared to more standard Vannier-type exciton relaxation in bulk material or singly nanocrystals.

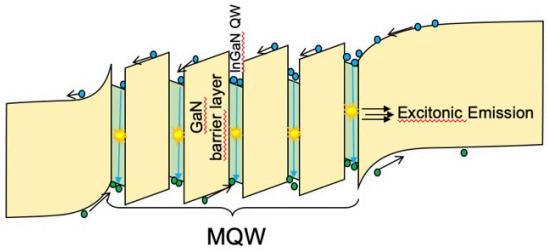

Fig. 28: Principle of eh pair creation and recombination in multiple quantum well structures. Courtesy of A. Hospodkova and M. Nikl, Czech Technical University of Prague.

Light yield values of the order of 100,000 photons/MeV can be expected, due to the small band gap of 3.3 eV and high binding energy of exciton, preventing charge delocalization and ionization losses.

An important technological challenge is to achieve sufficient total thickness of multiple quantum well structures to share a reasonable amount of the absorbed energy of incoming 511 keV photons and to suppress the slow defect emission, which competes with the fast excitonic one. However, important progress has been made to improve the production technology and up to 100 layers can be deposited now on sapphire substrates for a total thickness of 2 µm by Metal Organic Vapor Phase Epitaxy (MOVPE) (Fig. 29) [81].

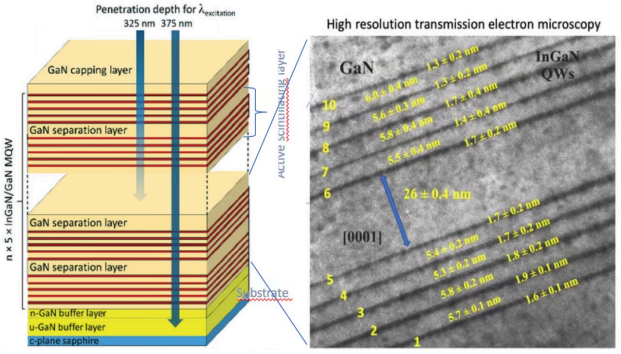

Fig. 29: Schematic of GaN/InGaN ultiple quantum well structures (left) and high resolution transmission electron microscopic image of a stack produced by MOVPE technology (right). Courtesy of M. Nikl, Czech Technical University of Prague. From [81].

5) Light transport with photonic crystals

The metascintillator concept offers a number of interesting possibilities to produce a bunch of prompt photons generated by a small energy leakage to nanocrystals or nanostructured quantum wells on top of the generally intense but slow scintillation pulse from standard dense scintillators. However, such nanostructures or nanocrystal layers are generally not transparent, and the problem of the fast light transport and collection by the photodetector needs to be solved.

Besides the possibility to host the nanocrystals in transparent plastic or MOF structures, the high potential of photonic crystals (PhC) to manage the behavior of optical photons is actively studied. In a perpendicular arrangement relative to the photodetector entrance face, PhCs can reorient the propagation modes, generally isotropic at the point of light emission into lateral propagation mode in the direction of the photodetector, reducing therefore the time jitter at the reception of these photons (Fig. 30).

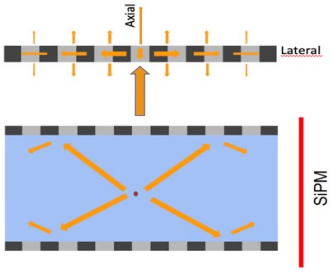

Fig. 30: PhC change of propagation mode from axial to lateral. Courtesy of L. Zhang, Multwace Metacrystal SA.

Different PhC designs have been simulated, using several approaches such as Rigorous Coupled Wave Analysis, Plane Wave Expansion, Guided Mode Expansion and Finite-difference time-domain methods, implemented in proprietary and open-source software. All these optical simulations demonstrate the ability of designed PhC slabs to bend light towards the metascintillator extraction surface, reducing the propagation modes and associated time jitter of photons within the scintillator. Choosing EJ232 plastic scintillator as the generator of prompt photons at a peak wavelength of 375 nm, different easy to produce materials have been investigated as a PhC substrate, such as Silica (SiO2), Gallium arsenide (GaAs) and Niobium pentoxide (Nb2O5), with nanostructuration patterns and dimensions compatible with the machining capabilities of available deposition and printing methods.

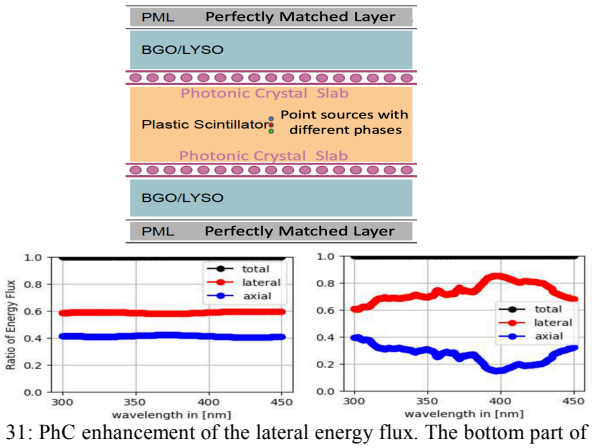

Fig. 31: PhC enhancement of the lateral energy flux. The bottom part of the figure shows the wavelength dependence of the fraction of the light flux traveling across the different scintillator layers (axial) and being directed laterally in the direction of the photodetector. The PhC produces a significant improvement at 400 nm. Courtesy of L. Zhang, Multwace Metacrystal SA.

Encouraging results have already been obtained with simple and not yet optimized designs, showing a significant gain of up

to 30% in the transmitted lateral energy flux toward the photodetector, opening the way to prototyping phases (Fig. 31).

V. Technologies for ≤100ps TOFPET resolution- Photodetectors and Si sensors

This section describes several ongoing efforts to understand the sources of time jitter in photo-detection and to improve the photodetector timing response (A). It also describes a PET scanner project using Si semiconductors for direct γ-tay detection instead of scintillators (B).

A. SiPM photodetectors

Photodetectors form an integral part of the scintillator-based gamma detector. They perform the crucial function of transforming physical quantities such as photon flow, into measurable and digitizable electrical ones, such as load and current. In the quest of fast timing, they are a paramount component that requires improvement in various aspects of their performance. While in the past different technologies, such as photomultiplier tubes (PMT) and avalanche photodiodes (APD) were mostly used, today the most relevant technology is based on silicon photomultipliers (SiPM), in analog or digital format [82].

Analog SiPMs have today the lead in production, testing and deployment in PET scanners. They are composed by an array of single photon avalanche detectors (SPADs), of size generally between 10 μm and 100 μm, connected in parallel to reach dimensions such as between 1x1 mm^2 and 6x6 mm^2. This way, they match the dimensions of most common pixel scintillator approaches, or provide a flexible spatial coverage and number of channels for monolithic detectors. For system integration, they are often packaged in arrays, that can be single or bi-dimensional. The digital SiPM case corresponds to coupling an independent read-out scheme for each SPAD or small group of SPADs. Research is performed to improve key specifications in both SiPM and SPAD level [83].

A key characteristic of SiPMs is their photon detection efficiency (PDE), composed by the quantum efficiency (QE) and fill factor of the silicon. Current state of the art reaches ~60% for LYSO scintillation wavelength peak [83, 84], a number that is expected to further improve, at least in the case of Hamamatsu S16 series (Fig. 32). Better PDE is indeed a critical parameter for timing resolution, which improves like the square root of the number of detected photons.

Another very important parameter when discussing timing, is the single photon time resolution (SPTR). This is at the moment a limiting factor to the CTR of optimized crystals, between 50 ps and 100 ps. Research on improving this is active and several approaches are being explored, such as masking the periphery of the SPAD, an area with electric field non-homogeneity and worse SPTR. An improvement of up to 50 ps has been observed for a 3x3x5 mm^3 BGO scintillator [85]. As SiPM SPTR deteriorates with the area of interconnected SPADs, because of a larger capacitance and increase dark noise, a possible solution can be the segmentation of the active area into small pixels, with separate readout, followed by signal summation or combination of time pick-off information.

Another significant improvement for SPTR comes from the field of nanophotonics, where the addition of hyperbolic metamaterials can restrict the conversion of the incoming photons to electron-hole pairs in well-defined regions of the SiPM structure, reducing therefore the jitter associated to the diffusion of the charge carriers to the avalanche region. A reduction of the STPR of FBK NUV-HD from 70 ps down to 10 ps is shown in simulations (Fig. 33) [86].

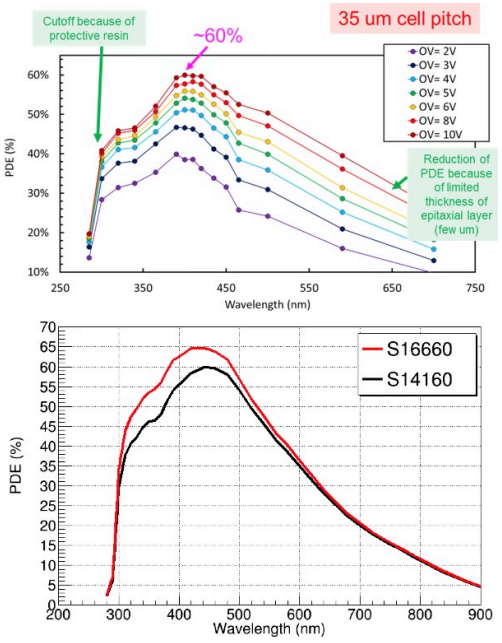

Fig. 32: (top) PDE over wavelength of FBK NUV-HD for different overvoltages [84]; and (bottom) comparison of PDE for S14 and S16 of Hamamatsu (courtesy of A. Gola, FBK and D. Castrillo, Hamamatsu).

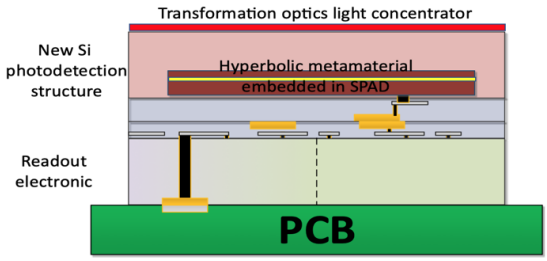

Fig.33: Schematic design of a SPAD enhanced with an embedded hyperbolic metamaterial layer. Courtesy of S. Enoch, Fresnel Institute. Marseille. From [86].

In the same direction, the design of metalenses, photonic structures focusing light similar to classical lenses, but without thickness, has been gaining momentum [87]. Metalenses are placed at the interface between scintillator and silicon. They are optimally coupled to both materials to maximize the optical transportation. Either applied in single SPADs (Fig. 34), or as in the case of [88, 89], attempted in a full MPPC SiPM (Fig. 35), metalenses seem to significantly improve SPTR. This comes at the cost of other key specifications of the system, such as DCR and cross-talk [90]. Research is ongoing to achieve better matching without sacrificing key aspects of the specifications.

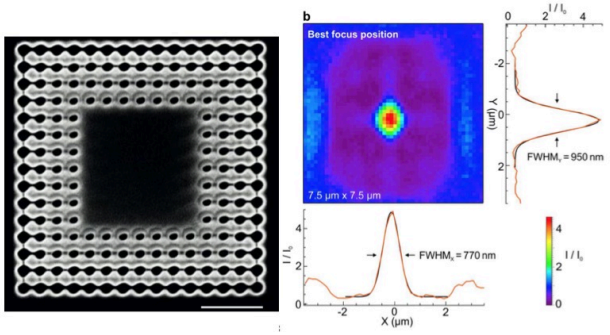

Fig. 34: (Left) printed metalens achieving focus of 80% of the light in less than 1x1 μm^2 at the center of the SPAD (right). Courtesy of S. Enoch, Fresnel Institute. Marseille . From [87].

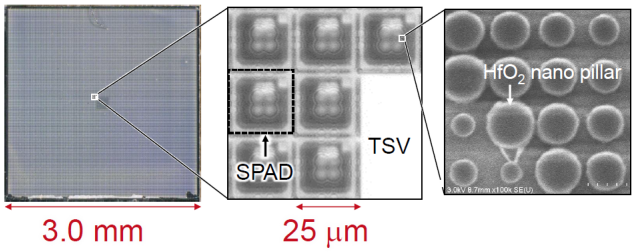

Fig. 35: A full 3x3 mm^2 MPPC diode (left) enhanced with surface metalenses, with 1:1 design coupling to independent 25x25 μm^2 SPADs (center), composed of variable size nanopillars (right). Courtesy of R. Ota, Hamamatsu. From [88].

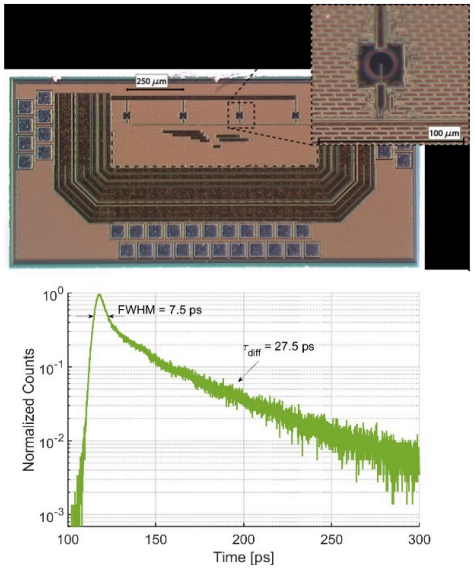

Fig. 36: (Top) SPAD design, embedded in a silicon circuit, for testing in optimal conditions; and (bottom) distribution of SPAD response, demonstrating a FWHM of 7.5 ps. Courtesy of C. Bruschini, F. Gramuglia and E.Charbon, EPFL, Lausanne. From [90].

Reduction of noise levels for silicon can be achieved through several ways, such as reducing the electronic background as well as minimizing the optical cross-talk between SPADs, and improving scintillator-SiPM optical coupling. New strategies such as implementing 3D and 2.5D through silicon vias (TSV) can also improve noise and SPTR. Direct TSV connection to digitizer ASICs can provide a full system-on-chip, with directly digitalized output and improved photodetector specifications. Finally, in order to allow read-out of optimized timing found in cross-luminescent scintillators such as BaF_2, expansion of SiPM sensitivity towards the vacuum-ultraviolet (VUV) area is ongoing, with current PDE in the order of 22% for 200 nm wavelength [60] and expectations for a factor of 2 improvement.

Work on single SPADs, in the direction of digital SiPM was reported by C. Bruschini, who showed some new interesting results, with an optimized design of a 25 μm diameter CMOS SPAD reaching a SPTR of 7.5 ps, for the first time reporting sub 10 ps timing in this field [90], (Fig. 36).

B. Direct γ-detection with Si semiconductor

A last but also interesting direction of development corresponds to the design of a pre-clinical PET system without scintillators, but with the use of semiconductor detectors (Fig. 37). These detectors are very commonly used in high-energy physics experiments or in modalities such as CT, as the possibility to design circuitry directly on the detector eliminates a lot of the inherent issues of scintillator detectors. The significant factors that have not yet allowed the adoption of such detectors for PET are related to the low stopping power of most semiconductors for the coincidence 511keV γ-rays, which are more energetic than X-rays commonly used in CT. In an effort to overcome this issue, the 100μPET project stacks 60 levels of silicon detectors, alone or interleaved with bismuth layers to improve stopping power. With a design of 100x100 μm^2 independent elements they reach a spatial resolution of around ~0.3 mm, close to or even beyond the positron range of most radiotracers [91]. This value significantly improves the signal-to-noise of the detector, as estimated in simulation. Time-of-flight capabilities are directly related to the power consumption, and it is not yet clear what value can be expected for 511 keV. However, in a high energy test beam environment this detector can reach below 100 ps timing resolution [91].

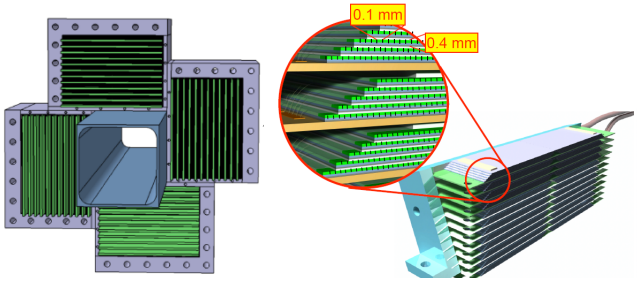

Fig. 37: Design of a pre-clinical PET system based on semiconductor detectors (left), composed of stacks of silicon circuits with sub-mm sizes (right). Courtesy of G. Iacobucci, University of Geneva.

VI. Technologies for ≤100ps TOFPET resolution: Electronics

The current efforts to improve the performance of crystals and light-sensors aiming at reaching the ultimate timing performance in PET applications, should be matched by equivalent progress in the electronics. A large effort is presently under way in the electronics front which was reflected in a dedicated and dense session of the workshop covering different

areas, in particular dedicated integrated circuits (A), low-power front-end implementations (B) and several system aspects (C).

A. Dedicated integrated circuits

Single channel PET electronics implemented with off-the-shelf components and using high-performance digital oscilloscopes have been developed by several groups achieving excellent performance [68, 69]. These electronics systems have been implemented mainly in the context of the development of new sensors, which require electronics with very good timing not compromising the measurement of the intrinsic sensor performance. These developments have also been useful to better characterize the bottlenecks in current PET electronics and to guide further developments of dedicated circuits. Indeed, it is clear that optimized top-bench implementations are not scalable to full PET scanners with many thousands of channels. This fact has motivated the development of several dedicated ASICs in the past years [92]. Two main categories of ASICs can be identified, namely full mixed-mode ASICs including the analog front-end and the digitization blocks, and pure analog circuits to be used in association with external TDCs. At the workshop, ASICs of each category were presented, which are among the most successful developments made by the PET research community.

TOFPET2 is a mixed-mode low-power (8 mW/channel) ASIC dedicated to PET developed by PETsys Electronics [93], which received considerable attention from the academic and industrial communities. Extensive literature on its performance has been published including comprehensive performance measurements [94]. At the workshop, the Aachen group discussed the timing limits of the TOFPET2 ASIC comparing CTR measurements obtained with an optimized electronics chain and with TOFPET2 [36]. LYSO:Ce crystals with dimensions 2x2x3 mm^3 and 3x3x20 mm^3 associated to photosensors HPK S14160-3050HS (3x3 mm^2, 50 µm SPADs) or Broadcom AFBR-S4N33C013 (3.14x3.14 mm^2, 30 µm SPADs) have been used. High frequency readout electronics adapted from [68] and [69], including BGA2803 amplifiers and the oscilloscope LeCroy WaveRunner 9404M-MS, bandwidth 4 GHz, 20 GS/s, have been used as reference [95]. Table I shows the results obtained. The best CTR obtained with HF readout electronics was 73 ps while with TOFPET2 it was 134 ps, which is slightly worse than reported in reference [94] in similar conditions (CTR=119 ps). The difference may be explained by different experimental conditions. This measurement indicates that TOFPET2 adds in quadrature about 100 ps to the CTR, which is larger than the CTR obtained with a single sensor connected to two ASIC channels (58 ps). The TOFPET2 TDC has a resolution of about 18 ps r.m.s. that explains this result. Further measurements reported at the workshop indicate that the degradation is possibly due to baseline fluctuations induced by dark counts.

The LIP-Lisbon group reported measurements obtained with the TOFHIR2 chip [96] developed for the new Timing Detector of the CMS experiment at CERN [97]. A block diagram of this ASIC is shown in Fig. 38. The analog implementation of the DLED algorithm [98] in TOFHIR2 is shown to stabilize the baseline and to reduce the effect of dark counts on the time resolution, providing an interesting avenue for improving the performance of dedicated ASICs for PET. The group reported a TOFHIR2 TDC resolution of 13 ps r.m.s. which translates in a contribution of 43 ps FWHM to CTR.

TABLE I
COMPARISON OF CTR MEASURED WITH HF READOUT ELECTRONICS AND WITH TOFPET2 (extracted from [36])

SiPM	Scintillator	$CTR_{SiPM+scintillator}$ / ps	$CTR_{TOFPET2}$ / ps
HPK S14160-3050HS	LYSO:Ce (EPIC) 3×3×20 mm^3	146 ± 2	200 ± 1
	LYSO:Ce (EPIC) 2×2×3 mm^3	91 ± 2	141 ± 2
Broadcom AFBR-S4N33C013	LYSO:Ce (EPIC) 3×3×20 mm^3	132 ± 2	203 ± 1
	LYSO:Ce (EPIC) 2×2×3 mm^3	**82 ± 2**	**142 ± 4**
	LYSO:Ce,Ca (TAC) 2×2×3 mm^3	73 ± 1	134 ± 10

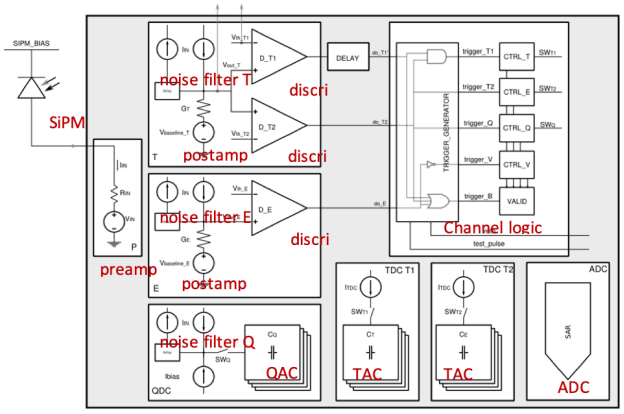

Fig. 38: Block diagram of the TOFHIR2 ASIC. Courtesy of J. Varela, LIP, Lisbon.

The IFIC group reported on advances in electronics for a Compton Camera [99]. The first readout system was based on the chip VATA64HDR16 from IDEAS. An alternative system with the ASIC TOFPET2 from PETsys Electronics was developed and evaluated including results in clinical beams showing spatial resolution of 4 mm. Improvements in several aspects were achieved with TOFPET2, in particular good energy resolution and timing resolution in CC mode.

The ICCUB Barcelona group reported on the FastIC ASIC developed in collaboration with the CERN Microelectronics group. FastIC is an analog 8 channel chip dissipating 12 mW/channel and providing energy and timing information encoded in output pulses that are processed by an external TDC [100]. Measurements with sensors HPK S13360 3050PE operated at 7 V overvoltage, associated to crystals LSO:Ce Ca 0.2% of 2x2x3 mm^3, yield CTR of 94 ps (Fig. 39). This result is slightly better than the performance of the TOFPET2 frontend of around 104 ps, obtained by subtracting in quadrature the TDC contribution to the CTR. It is worth noting that the negative effect of dark counts in TOFPET2 does not allow to work with SiPM over-voltage above 4 V without severe degradation of the time resolution. An improvement of this aspect in future versions would certainly be welcome.

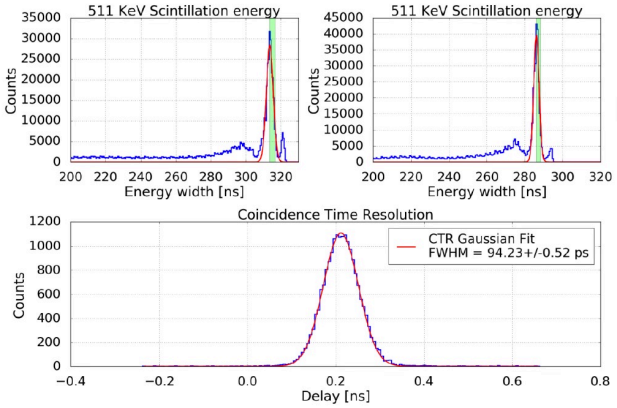

Fig. 39: CTR measurement of the FastIC with LSO:Ce Ca 0.2% measuring 2 × 2 × 5 mm3 coupled to a HPK S13360-3050CS SiPM at 7 V of over-voltage. 10 K events have been used in coincidence to compute the CTR. Courtesy of D. Gascon, UCCUB, Barcelona. From [100].

B. *Low power implementations*

The LBNL group presented a low power implementation of high-performance electronic readout for TOFPET, exploiting the use of a small footprint Balun transformer and a cascade of RF amplifiers, maximizing bandwidth, gain and pulse slew rate. The use of Balun transformer was shown to minimize the negative effect of the high capacitance of large area SiPMs that reduces pulse amplitude and slew rate. The group implemented the circuit shown in Fig. 40 in a PCB with footprint of the order of 3x16 mm^2, which achieves SPTR of 95 ps (FWHM) in association with the SiPM Broadcom S4N33C013 3x3 mm^2 operated at 10V over-voltage, with a power consumption of 10 mW. Using 20 mm long LYSO crystals and the same SiPM, the circuit achieves CTR of 127 ps with the RF amplifiers at maximum voltage (power 60 mW) and the waveforms digitized at 40 GSa/sec. These are remarkable results. Nevertheless, the implementation is hardly scalable to large PET systems given the large PCB area per channel (roughly a factor 20 larger than TOFPET2, for example).

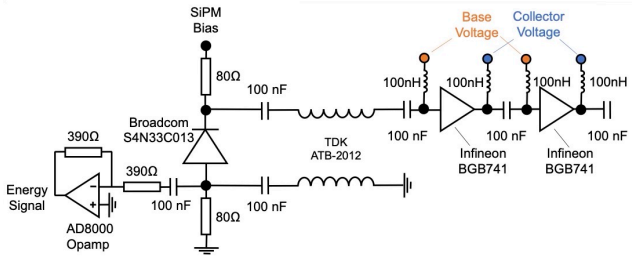

Fig. 40: Front-end design based on micro-balun transformer and low noise monolithic microwave integrated circuits. Courtesy of J. Cates, LBNL, Berkeley.

A similar approach has been followed by a collaboration of Multiwave-Metacrystal and I3M to minimize the power consumption for Time-of-Flight PET SiPM readout. Several Balun transformer types were exploited. In general, 15-20% improvement between 1:1 and 1:2 balun impedance ratio was observed (Table II). Power efficient implementations have also be studied in [95].

TABLE II
COMPARISON OF TIMING PERFORMANCE FOR DIFFERENT BALUN RATIOS AND TIMING AMPLIFICATION STAGES (TAS).

CTR MEASUREMENTS				
Number of TAS	no TAS		1 TAS	
Balun Ratio	1:1	1:2	1:1	1:2
Semi-ideal	27 ps	23 ps	8 ps	5 ps
Crystal	131ps	118 ps	104 ps	91 ps

The group of the Seoul National University conducted a comparative study on various capacitance compensation techniques for SiPM based TOF-PET detectors. In particular, circuits exploiting the negative Miller effect (Fig. 41) showed 38% improvement in CTR.

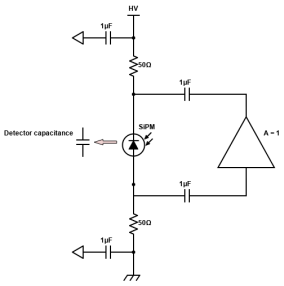

Fig. 41: Circuit exploiting the negative Miller effect. Courtesy of Hyeong Seok Shim and Jae Sung Lee, Seoul National University.

The Forschungszentrum in Jülich presented an ambitious program aiming at the design of high speed and low noise receiver electronic systems. One approach is to improve the input stage of the TOFPET2 ASIC, introducing an input amplifier with a HF bandwidth and a pole zero filter to reduce baseline shifts. The group intends to scrutinize two concepts, namely an ASIC for analog SiPMs, and smart SPAD based 3D integrated image sensor.

C. *System aspects*

Aiming at ultimate performance in time extraction requires the implementation of time walk corrections to compensate the dependence of the time measurement on the pulse amplitude. The correction is normally a simple function of the pulse energy. The group from Seoul National University investigated the use of high-frequency sampling (5 GS/s) of the pulse rising edge as input to a neural-network based feature extraction algorithm named Dynamic Threshold Discriminator (DTD). It was shown that the DTD algorithm outperforms the usual methods (Fig. 42).

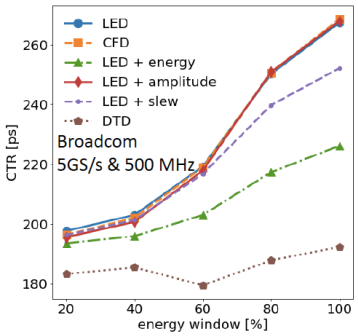

Fig. 42. CTR as a function of the energy window for different time extraction algorithms. The results were obtained with 3×3×20 mm^3 LYSO:Ce:Mg crystals associated to Broadcom SiPMs and the HF frontend circuit described in [101]. Courtesy of S. Bae, Seoul National University.

High-performance timing in PET systems could be exploited in non-usual ways. The group of the Ghent University in collaboration with Molecubes has investigated time-based event positioning in monolithic detectors. A simulation study showed that Time-over-Threshold (ToT) information of each channel provides good positioning accuracy (Fig. 43). The group concluded that ToT readout can be a valuable and high performant alternative for monolithic PET detectors.

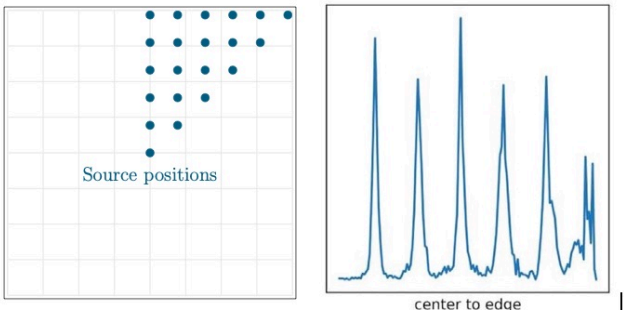

Fig. 43: Simulation of the event positioning in a monolithic detector with a 8x8 array using ToT information. Courtesy of C. Thyssen and S. Vandenberghe, Ghent University.

VII. New Approaches for Improving TOFPET Performance: Artificial Intelligence and Image Reconstruction

Progress in fast timing will have an impact on image reconstruction and require more and more artificial intelligence (AI) features to deal with a much richer information provided by the detectors. This is certainly true for the paradigm shift introduced by the 10ps TOFPET challenge and the reconstruction-free PET described in sub-section A. More generally, sub-section B discusses the increasing role of AI for the position and timing resolution in PET scanners. The growing importance of AI for image denoising is shown in subsection C, whereas sub-section D addresses the possibilities offered by AI for fast prototyping.

To reach still better coincidence time resolutions, many different detector types are being investigated, as was illustrated in every session of the workshop, including this one [102, 103]. Some of these detectors have an event-dependent time resolution, and new analysis tools are needed to determine the value of such systems for image reconstruction [104, 105, 106, 107]. When the TOF resolution will approach or even exceed the spatial detector resolution, angular sampling is no longer mandatory [102] and novel algorithms for reconstructing the final clinical images will be needed [102, 112]. This is illustrated with a proof of principle prototype developed at UC Davis [109], which is described below.

As is the case in many other fields, artificial intelligence has a continuously increasing impact on TOF-PET imaging. It is being used in the front-end electronics to improve the estimation of the exact location and time at which the gamma photon interacted with the detector [102, 108, 110, 111], it is used for noise suppression during or after image reconstruction [110], and as a fast surrogate for computations which can be done exactly but require excessive computation times [103].

A. The value of high TOF resolution

The proof-of-principle of a TOFPET system with a 32 ps FWHM coincidence time resolution (CTR) has been implemented with 2 lead glass detectors and validated in [102, 109] as discussed in section II C. This CTR corresponds to a spatial resolution of 4.8 mm FWHM along the line of response (LOR), very similar to the detector resolution perpendicular to the LOR. A convolutional neural network (CNN) takes the pair of digitized waveforms as the input, and outputs the estimate of the gamma interaction time. For this prototype, two collimated detectors were used to acquire a single LOR, and by shifting this detector pair in 1 mm steps, a set of parallel LORs through a slice was obtained. Fig. 44 shows a result obtained on a phantom with diameter of 30 mm, using a collimation of 2 mm inside the slice and 10 mm perpendicular to the slice. The system is called a direct positron emission imager (dPEI) because of its excellent TOF resolution of 32 ps, allowing each event to be immediately assigned to a single pixel in the image (with a spatial resolution of 4.8 mm). Current post-processing includes correction for attenuation, sensitivity, radioactive decay and acquisition time. For clinical systems, also scatter correction will have to be included. In lead glass, on average 8.7 Cherenkov photons are produced. A newly designed detector is using BGO crystals (with a high stopping power and better energy resolution than lead glass and 15.6 i.e.2 times more Cherenkov photons), sandwiched between the MCP-PMT and a SiPM. Its current CTR is 40 ps FWHM in this configuration. In future designs, the collimated detectors will of course be replaced by 2D detector arrays, to increase the sensitivity dramatically.

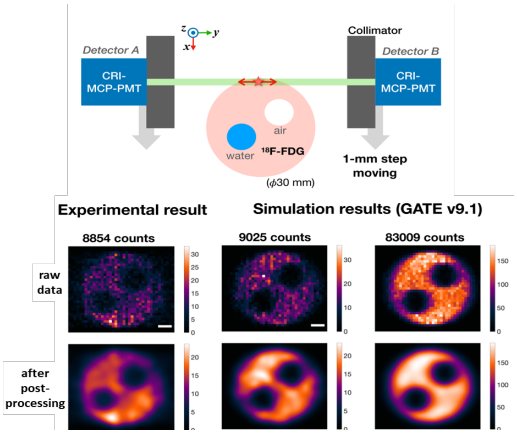

Fig. 44: Row 1: the Cherenkov radiator integrated MCP-PMT (CRI-MCP-PMT) detectors acquired points-of-response (PORs) on a given *x*-position and scan along the *x*-axis to generate a cross-sectional image slice on the *xy*-plane. Row 2: raw experimental and simulation data. Row 3: corresponding post-processed images. The scale bar is 5 mm long. Courtesy of Sun Il Kwon, UC Davis. From [102].

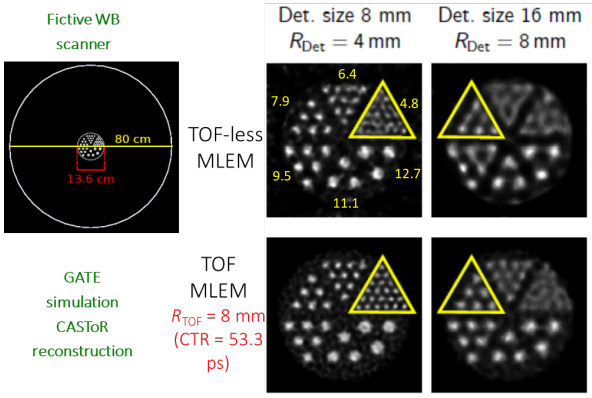

Fig. 45: GATE simulation of an 80 cm diameter 2D PET scanner, acquiring an image of a 13.6 cm diameter phantom, containing 6 groups of rods with diameters ranging between 4.8 mm and 12.7 mm. MLEM reconstructions from non-TOF and 8 mm TOF are shown for detectors of 8 and 16 mm. Courtesy of Roger Lecomte. Slightly modified from [112].

R. Lecomte et al [112, 113] have performed 2D Monte Carlo simulations of TOF-PET systems with complete angular sampling, and with very high TOF resolutions. They show that when the TOF resolution is superior to the spatial detector resolution, the resolution of the reconstructed image is determined by the TOF resolution. Further, since the acollinearity blurring is perpendicular to the LOR, the TOF-resolution along the LOR is not affected by it. Since, even in 2D TOF-PET, the acolinearity for a single emission point can be probed in all the planes around a given LOR, the acollinearity blurring is compensated in all directions by the TOF-resolution. For the same reason, in such TOF-systems, good resolution images can be obtained with much larger detectors. In addition, because TOF increases the effective sensitivity and accelerates the convergence of the MLEM algorithm, high resolution low noise images can be achieved with ultra-high TOF-MLEM, whereas non-TOF MLEM reconstructions from the same data are noisy and blurred. This is illustrated in Fig. 45, where the TOF reconstructions are much sharper than the non-TOF ones, although the TOF resolution of 8 mm FWHM is not even superior to the detector resolutions (4 and 8 mm FWHM).

In [104], the gain in signal to noise ratio (SNR) provided by TOF was analytically computed for two different tasks. One task was the detection of the presence of a small hot spot in the center of an arbitrary tracer distribution in a signal-known-exactly / background-known-exactly setting. The other task was the achieved SNR in the center of the reconstructed image from the TOF-PET scan of a uniform cylinder. It was found that with good approximation, the SNR gain due to TOF was identical for the two tasks. It is given by

$$\frac{SNR^2_{TOF}}{SNR^2_{nonTOF}} = D\int_{a-\infty}^{\infty} k^2(x)dx$$

where D is the diameter of the cylinder and $k(x)$ is the TOF-kernel. For a Gaussian TOF-kernel, the result is identical to the well-known expression derived by Tomitani [7]. This result generalizes Tomitani's derivation to TOF-kernels of arbitrary shape; it can be used to rank TOF-PET systems having a distribution of (event-dependent) non-Gaussian TOF-kernels, as encountered, amongst others, in metascintillators and mixed Cherenkov-scintillation detectors.

B. Artificial intelligence for improving the position and timing resolution in PET detectors

Monolithic detectors are receiving increasing attention, because they can achieve high sensitivity, good DOI and excellent spatial resolution. However, their timing performance is less impressive. Because effective training data can be produced with both simulations and experiments, the estimation of the interaction time and position is an excellent problem for convolutional neural networks (CNN). Belcari *et al.* proposed an AI boosted 4D positioning algorithm for their UTOFPET system [108, 114]. A monolithic LYSO crystal is connected to an 8 × 8 SiPM array. A 3D positioning CNN takes the 256 charges recorded by the SiPMs as input. In addition, a few "engineered" features are inserted at the last layer. These features include the number of pixels with a signal above a particular threshold, and the estimated width of the scintillation light spot. These features should help the network to recognize the DOI. The CNN outputs the x, y and z coordinates of the estimated interaction point in the crystal. A very similar CNN is used to estimate the event interaction time. The inputs for this CNN are the same 256 charges and the 256 SiPM timestamps, and no engineered features. The outputs of both CNNs are combined and refined by a last layer, as illustrated in Fig. 46.

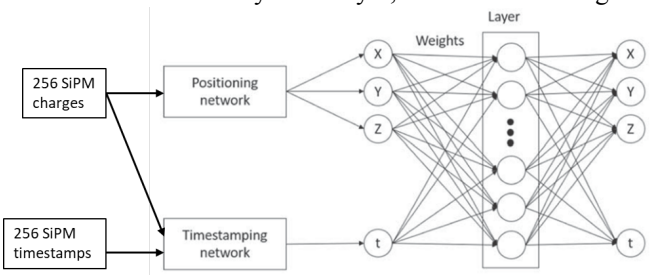

Fig. 46: The 4D positioning CNN, driven by an 8 x 8 array of SiPMs. Slightly modified from [108]. Courtesy of N. Belcari, INFN Pisa.

The network is trained with a combination of experimental data and simulations (using Geant4 for optical and analytical

models for SiPM simulation). It is found that all four outputs x, y, z and t benefit from the refinement layer, and in particular the z coordinate is highly relevant for timing estimation. The results also benefit from adding simulation data to the training data.

Vandenberghe, Maebe *et al.* [110, 111] proposed a related approach for estimating the interaction time, which they call a "3D-CNN". This CNN takes a three-dimensional input of 8 × 8 SiPMs × 31 waveform samples per SiPM. The method was evaluated with simulations, using GATE for gamma and optical photons simulation and bi-exponential functions for simulating the SiPM. They report that using discretized waveforms instead of a single time stamp from each SiPM improves the accuracy of the final interaction time estimate, with an excellent uniformity of the time resolution over the crystal, in particular along the DOI axis. The temporal sampling of the waveforms was not critical, the results with 5 Gsamples/s were only slightly inferior to those with 20 Gsamples/s. Fig. 47 shows that the 3D-CNN outperforms the 2D-CNN (using single time stamps instead of 31 waveform samples), which in turn outperforms averaging SiPM time stamps.

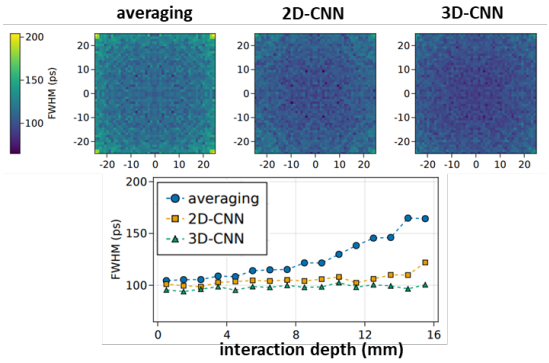

Fig. 47: The results of the 3D positioning CNN, driven by an 8 x 8 array of SiPMs with 31 waveform samples per SiPM. The images show the DTR as a function of 2D position. The plot shows the DTR as a function of DOI. Courtesy of J. Maebe, Ghent University. From [111].

In [105], the information provided by the first N optical photons detected in the SiPM was estimated. Monte Carlo simulations of the generation and propagation of Cherenkov and scintillation photons in a BGO crystal ($3\times3\times20$ mm^3) were performed. When the photons entered the SiPM, immediate detection was assumed. A maximum likelihood algorithm was implemented to estimate the 511 keV photon interaction time from the arrival times of the first N optical photons. The method was applied to determine the effect of the average number of detected Cherenkov photons on the DTR. Currently, on average 3.24 of the 17 emitted Cherenkov photons are detected. It was found that modest increases to 4 and 6 detected photons improved the standard deviation of the DTR from 106 ps to 79 and 49 ps. As the number of detected Cherenkov photons increases, there is more benefit in using a larger number N of first photons in the maximum likelihood estimation.

C. *AI for noise suppression*

Human observers' performance is better predicted with channelized-Hotelling observers than with the Hotelling observer [115], implying that the human visual system does not optimally deal with correlated noise. That is why lesion detection by human experts improves when moderate regularization is applied to reduce the noise on the images, although the regularization actually reduces the information in the image. Many researchers report that image denoising with deep learning methods usually outperforms handcrafted denoising approaches, and CNN-based denoising is becoming very popular in medical imaging [110]. Training is usually done with matched low noise and high noise image pairs. An example is given in [116], where a CNN is trained to predict TOF-PET images from reconstructed non-TOF-PET images.

D. *AI for fast prototyping*

Finally, I. Pan *et al.* studied the combination of AI and uncertainty quantification (UQ) as a fast alternative to Monte Carlo simulations [103]. When Monte Carlo simulations are used to optimize design parameters (e.g. designing a metascintillator), the computational burden is enormous. To reduce this burden, the generation of a large number of Monte Carlo samples is replaced with the computation of a small number of UQ samples. For UQ, non-intrusive polynomial chaos expansion was used to propagate the uncertainty on the input. This approach essentially models the output of the Monte Carlo simulator based on a polynomial expansion. The polynomial coefficients are determined by maximizing agreement with Monte Carlo simulated samples. In the optimization, the choice of the next sample point is determined by a machine learning model, which learns during the optimization, see Fig. 48. Acceleration factors of around five have been obtained [103].

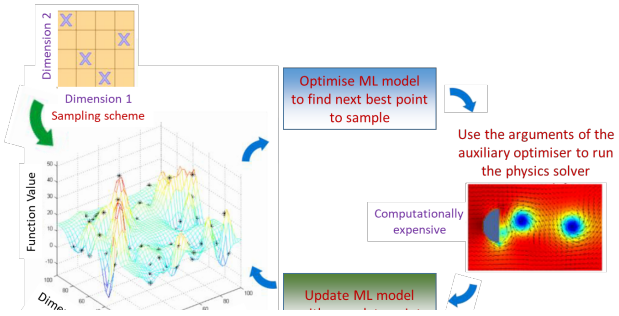

Fig. 48: The machine learning surrogates-based optimization with embedded UQ (UQ part is not shown in the above schematic).). Slightly modified from [103]. Courtesy of I. Pan, Quaisr..

VIII. CONCLUSIONS

The quest for ultimate TOFPET performance is a vibrant multidisciplinary research area, involving experts in the different components of the complex information chain, from the precise 4D determination of the interaction of the 511keV γ-rays resulting from the positron annihilation, to the image reconstruction and extraction of the clinical information. The workshop: Fast Timing in Medical Imaging, organized in June 3-5, 2022 in Valencia (Spain), was an opportunity to gather more than 100 of these experts worldwide and to make a status of the impressive progress made in the different domains concerned: scintillators, photodetectors, readout electronics,

image reconstruction, artificial intelligence. The clinical relevance for pushing the TOF resolution from nearly 200 ps, the state-of-the-art today at a system level, to 100 ps in a first step, and going in the direction of 10 ps on a longer term, has been considered very high and is pushing for a convergence of the efforts in all these different domains for reaching this very ambitious goal for cost effective fully integrated TOFPET scanners. This paper can be considered as an update of the "Roadmap toward the 10ps time-of-flight PET challenge" [1] two years after its publication.

ACKNOWLEDGEMENTS

This workshop has been partially funded by the Conselleria de Innovación, Universidades, Ciencia y Sociedad Digital, belonging to the Generalitat Valenciana, under grant CIAORG/2022/92. Additional thanks are also going to our other sponsors, Multiwave Metacrytsal SA., Crystal Photonics Inc., Epic-Crystal, Hamamatsu, Molecubes and Bruker.

The authors would like to thank all the participants for their contribution to the workshop, with their presentations but also the very interesting discussions, which provided a rich material for this paper. We are also thankful to the organization committee, and in particular to A. Gonzalez-Montoro and J. Barrio from I3M, as well as to P. Sanjuez and her team from Valenciatur events.

REFERENCES

[1] P. Lecoq, C. Morel, J. Prior et al . "Roadmap toward the 10ps time-of-flight PET challenge", *2020 Phys. Med. Biol.* **65** 21RM01.

[2] T. Carlier et al., "From a PMT-based to a SiPM-based system: a study to define matched acquisition/reconstruction parameters an NEMA performance of the Biograph Vision 450", EJNMMI Physics (2020) 7:55

[3] https://the10ps-challenge.org

[4] M. Ter-Pogossian et al., "Photon time-of-flight assisted positron emission tomography", *J. Comput. Assist. Tomogr. 5:227-239.1981*

[5] R. Allemand et al., "Potential Advantages of a Cesium Fluoride Scintillator for a Time-of-Flight Positron Camera", *J. Nucl. Med., February 1980, 21 (2) 153-155.*

[6] NA. Mullani, WH. Wong et al., "Design of TOFPET: a high-resolution time-of-flight positron camera", *Proceedings of the International Workshop of Time-of-Flight Positron Tomography; St. Louis, Missouri; May 1981.*

[7] T. Tomitani, "Image reconstruction and noise evaluation in photon time-of-flight assisted positron emission tomography", *IEEE Trans. Nucl. Sci. vol.28, pp. 4582-4588,1981.*

[8] T. Budinger, "Time-of-Flight Positron Emission Tomography: Status Relative to Conventional PET", *J. Nucl. Med., January 1983, 24 (1) 73-78.*

[9] H. Cramer, "Mathematical Methods of Statistics", *Princeton Univ. Press 1946, ISBN 0-691-08004-6. OCLC 185436716.*

[10] G. Razdevšek et al., "Multi-panel limited angle PET system with 50 ps FWHM coincidence time resolution: a simulation study," i*IEEE TRPMS*, 2021.3115704.

[11] SI. Kwon et al., "Ultrafast timing enables reconstruction-free positron emission imaging*", Nature Photonics volume 15, pages 914–918 (2021).*

[12] SI. Kwon et al., "Dual-ended readout of bismuth germanate to improve timing resolution in time-of-flight PET", *2019* Phys. Med. Biol. ***64*** *105007.*

[13] G. Arino-Estrada et al., "First Cherenkov charge-induction (CCI) TlBr detector for TOF-PET and proton range verification", 2019 *Phys. Med. Biol.* 64 175001.

[14] E. Ł. Stępień, C. Rząca, and P. Moskal, "Novel biomarker and drug delivery systems for theranostics – extracellular vesicles," *Bio-Algorithms and Med-Systems,* vol. 17, no. 4, pp. 301-309, 2021, doi:10.1515/bams-2021-0183.

[15] P. Lecoq, "Pushing the Limits in Time-of-Flight PET Imaging," *IEEE Transactions on Radiation and Plasma Medical Sciences,* vol. 1, no. 6, pp. 473-485, 2017, doi: 10.1109/TRPMS.2017.2756674.

[16] N. Kratochwil et al., "A roadmap for sole Cherenkov radiators with SiPMs in TOF-PET", *Phys. Med. Biol. 66 195001.*

[17] G. Terragni et al., "Time Resolution Studies of Thallium Based Cherenkov Semiconductors", *Frontiers in Physics, Sec. Radiation Detectors and Imaging.*

[18] N. Kratochwil et al., "Pushing Cherenkov PET with BGO via coincidence time resolution classification and correction", *Phys. Med. Biol. 65 115004*

[19] S. Gundacker et al, "Precise rise and decay time measurements of inorganic scintillators by means of X-ray and 511 keV excitation" Nuclear Inst. and Methods in Physics Research, A 891 (2018) 42–52.

[20] V. Nadig, et.al, "A comprehensive study on the timing limits of the TOFPET2 ASIC and on approaches for improvements", IEEE Trans. Rad. Plasma Med. Scie. 2022.

[21] N. Cucarella et al, "Timing evaluation of a PET detector block based on semi-monolithic LYSO crystals", Med Phys., **48**, 8010–8023, (2021). https://aapm.onlinelibrary.wiley.com/doi/full/10.1002/mp.15318.

[22] P. Lecoq, "Development of new scintillators for medical applications", Nucl. Instrum. Methods A 809, 130–139, 2016.

[23] R.M. Turtos et al, "Towards a metamaterial approach for fast timing in PET: an experimental proof-of-concept", *Phys. Med. Biol*., **64,** 185018, (2019).https://doi.org/10.1088/1361-6560/ab18b3.

[24] P. Lecoq et al., Metascintillators: New results for TOFPET applications, IEEE Trans. Radiat. Plasma Med. Sci., 1–1, 2022.

[25] G. Konstantinou, P. Lecoq, J. M. Benlloch, and A. J. Gonzalez, "Metascintillators for Ultrafast Gamma Detectors: A Review of Current State and Future Perspectives", IEEE Trans. Rad. Plasma Med. Scie. 6, 5–15, 2022.

[26] F. Pagano et al, "Advances in heterostructured scintillators: toward a new generation of detectors for TOF-PET", *Phys. Med. Biol*., **67,** 135010, (2022).https://doi.org/10.1088/1361-6560/ac72ee..

[27] N.Z. Yussefian, et al., "TOF Benefits and Trade-offs on Image Contrast-to-Noise Ratio Performance for a Small Animal PET Scanner", IEEE Trans. Rad. Plasma Med. Scie. 6, 687, 2021.

[28] C. Valladares, et al., "Evaluation of Crystal Arrays for Accurate Positioning and Timing PET detectors", IEEE NSS MIC conference proceeding 2021.

[29] J. W. Cates and C. S. Levin, "Evaluation of a clinical TOF-PET detector design that achieves 100 ps coincidence time resolution," *Phys Med Biol,* vol. 63, no. 11, p. 115011, Jun 7 2018, doi: 10.1088/1361-6560/aac504.

[30] S. Pourashraf *et al.*, "Scalable electronic readout design for a 100 ps coincidence time resolution TOF-PET system," *Phys Med Biol,* vol. 66, no. 8, Apr 14 2021, doi: 10.1088/1361-6560/abf1bc.

[31] P. Moskal *et al.*, "Simulating NEMA characteristics of the modular total-body J-PET scanner-an economic total-body PET from plastic scintillators," *Phys Med Biol,* vol. 66, no. 17, Sep 1 2021, doi: 10.1088/1361-6560/ac16bd.

[32] P. Moskal and E. L. Stepien, "Prospects and Clinical Perspectives of Total-Body PET Imaging Using Plastic Scintillators," *PET Clin,* vol. 15, no. 4, pp. 439-452, Oct 2020, doi: 10.1016/j.cpet.2020.06.009.

[33] M. Jacquet *et al.*, "A time-of-flight-based reconstruction for real-time prompt-gamma imaging in proton therapy," *Phys Med Biol,* vol. 66, no. 13, Jun 22 2021, doi: 10.1088/1361-6560/ac03ca.

[34] J. Rossignol *et al.*, "Time-of-flight computed tomography - proof of principle," *Phys Med Biol,* vol. 65, no. 8, p. 085013, Apr 22 2020, doi: 10.1088/1361-6560/ab78bf.

[35] D. Gaudreault, J. Rossignol, Y. Bérubé-Lauzière, and R. Fontaine, "Comparative Study of Image Quality in Time-Correlated Single-Photon Counting Computed Tomography," *IEEE Transactions on Radiation and Plasma Medical Sciences,* vol. 5, no. 3, pp. 343-349, 2021, doi: 10.1109/TRPMS.2020.3017702.

[36] A. Vasiliev, "Relaxation of hot electric excitations in scintillators: account for scateering, track effects, compicatd electronic structure", proceeding of the Scint99 conference, Moscow 1999, 43-52.

[37] E. Auffray et al., "A Comprehensive & Systematic Study of *Coincidence Time Resolution* and *Light Yield* Using Scintillators of Different Size and Wrapping", IEEE Transactions on Nuclear Science, Vol 60 ,(5) , 2013 , pp. 3163 – 3171.

[38] M. Nikl et al, "Modification of $PbWO_4$ scintillator characteristics by doping", J.Cryst. Growth **229**, 312-315 (2001)

[39] M. Nikl, et al, "The doping of $PbWO_4$ in shaping its scintillator characteristics", Radiation Measurements **33**, 705-708 (2001)

[40] A. Annenkov, M. Korzhik, P. Lecoq, "Lead tungstate scintillation material", Nucl. Instrum. Methods Phys. Res. A 490 (2002) 30–50.

[41] M. Korzhik et al., "Ultrafast PWO scintillator for future high energy physics instrumentation", Nucl. Instrum. Methods Phys. Res. A 1034 (2022)166781

[42] M. A. Spurrier et al., "Effects of Ca^{2+} Co-Doping on the Scintillation Properties of LSO:Ce," IEEE Transactions on Nuclear Science, vol. 55, no. 3, 2008 pp.1178–1182.

[43] H. E. Rothfuss et al., "The Effect of Ca^{2+} Codoping on Shallow Traps in YSO:Ce Scintillators," IEEE Transactions on Nuclear Science, vol. 56, no. 3, 2009 pp. 958–961,

[44] S. Blahuta et al. "Evidence and Consequences of Ce4+ in LYSO:Ce,Ca and LYSO:Ce,Mg Single Crystals for Medical Imaging Applications," IEEE Transactions on Nuclear Science, vol. 60, no. 4, 2013. pp. 3134–3141,

[45] M. Nikl et al. "Defect Engineering in Ce-Doped Aluminum Garnet Single Crystal Scintillators," Crystal Growth & Design, vol. 14, no. 9, 2014, pp. 4827–4833

[46] M. Nikl and A. Yoshikawa, "Recent R&D Trends in Inorganic Single-Crystal Scintillator Materials for RadiationDetection," Advanced OpticalMaterials, vol. 3, no. 4, 2015, pp. 463–481,

[47] K. Kamada, M. Nikl, S. Kurosawa, A. Beitlerova, A. Nagura, Y. Shoji,J. Pejchal, Y. Ohashi, Y. Yokota, and A. Yoshikawa, "Alkali earth cooping effects on luminescence and scintillation properties of Ce doped $Gd_3Al_2Ga_3O_{12}$ scintillator," Optical Materials, vol. 41, 2015, pp. 63–66,

[48] M. T. Lucchini, V.Babin, P.Bohacek, S.Gundacker, K.Kamada,M.Nikl, A.Petrosyan, A.Yoshikawa and E.Auffray, "Effect of Mg^{2+} ions co-doping on timing performance and radiation tolerance of cerium doped $Gd_3Al_2Ga_3O_{12}$ crystals", Nucl. Instr. Meth. Phys. Res. A 816, 2016, 176–183.

[49] M. Korzhik, V. Alenkov, O. Buzanov, G. Dosovitskiy, A. Fedorov, D. Kozlov, V. Mechinsky, S. Nargelas, G. Tamulaitis and A. Vaitkevičius, "Engineering of a new single-crystal multiionic fast and high-light-yield scintillation material $(Gd_{0.5}Y_{0.5})_3Al_2Ga_3O_{12}$:Ce,Mg". CrystEngComm 22, 2020, 2502–2506.

[50] L. Martinazzoli, S.Nargelas, P. Bohacek, R. Cala', M. Dušek, J. Rohlíek, G. Tamulaitis, E. Auffray and M. Nikl, "Compositional engineering of multicomponent garnet scintillators: Towards an ultra-accelerated scintillation response" Mater. Adv. 2022, DOI: 10.1039/D2MA00626J

[51] P. Hohenberg and W. Kohn, "Inhomogeneous Electron Gas ", Phys. Rev. **136**, B864 – Published 9 November 1964

[52] M. G. Brik and A. M. Srivastava, "Ab initio studies of the structural electronic and optical properties of K_2SiF_6 single crystals at ambient and elevated hydrostatic pressure", *J. Electrochem. Soc.*, vol. 159, no. 6, pp. .J212-J216, 2012.

[53] O Salawu, O Bouhali, "Defect process in bismuth germanante: A precursor to band-edge engineering and design of stable scintillators", Bulletin of the American Physical Society, 2022

[54] C. W. E. Van Eijk, "Cross-luminescence", Journal ol Lurninescence 60, 1994, 936-941

[55] P. Rodnyi, M. Terekhin and E. Mel'chakov, "Radiative core-valence transitions in barium-based fluorides" J. Lumin. 47 1991, 281–284

[56] E. Radzhabov, M. Kirm, A. Egranov, A. Nepomnyachshikh and A. Myasnikova, A mechanism of exciton suppression in alkaline-earth fluorides doped with La, Y, Cd", 2006, Proc. SCINT 2005. 60-63

[57] J. Chen, et al., "Development of Yttrium Doped BaF2 Crystals for Future HEP Experiments", *IEEE Trans. Nucl. Sci., vol. 65, no. 8, 2018, 2147-2151,*

[58] S. Gundacker et al., "Vacuum ultraviolet silicon photomultipliers applied to BaF_2cross-luminescence detection for high-rate ultrafast timing applications", Phys. Med. Biol. 66 (2021) 114002

[59] J. Saaring, E. Feldbach, V. Nagirnyi, S. Omelkov, A. Vanetsev and M. Kirm, "Ultrafast Radiative Relaxation Processes in Multication Cross-Luminescence Materials," in *IEEE Transactions on Nuclear Science*, vol. 67, no. 6, 2020, 1009-1013, doi: 10.1109/TNS.2020.2974071.

[60] V. Vanecek, J. Páterek, R.Král, R.Kučerková, V.Babin, J.Rohlíček, R.Cala', N.Kratochwil, E.Auffray, M.Nikl, "Ultraviolet cross-luminescence in ternary chlorides of alkali and alkaline-earth metals", Optical Materials X 12 (2021) 100103.

[61] P. Lecoq et al., "Can transient phenomena help improving time resolution n scintillators", IEEE TRans. Nucl. Sc. Vol. 61, N°1, Feb. 2014.

[62] L. Tao, R. N. Coffee, D. Jeong, and C. S. Levin, "Ionizing photon interactions modulate the optical properties of crystals with femtosecond scale temporal resolution," *Phys Med Biol,* vol. 66, no. 4, p. 045032, Feb 12 2021, doi: 10.1088/1361-6560/abd951.

[63] G. Tamulaitis, A. Vasil'ev, M. Korzhik, A. Mazzi, A. Gola, S. Nargelas, A. Vaitkevičius , A. Fedorov, and D. Kozlov, Improvement of the Time Resolution of Radiation Detectors Based on Gd3Al2Ga3O12 Scintillators with SiPM Readout, IEEE Trans. Nucl. Sci. 66, (2019),1879 .

[64] S. Nargelas, G. Dosovitskiy, M. Korzhik, G. Tamulaitis, Role of inter- and intraconfigurational transitions of Pr^{3+} ion in nonequilibrium carrier relaxation in garnet-type scintillators, Optical Materials, 111, (2021), 110676.

[65] S. Nargelas, Y. Talochka, A. Vaitkevičius, G. Dosovitskiy, O. Buzanov, A. Vasil'ev, T. Malinauskas, M. Korzhik, G. Tamulaitis, Influence of matrix composition and its fluctuations on excitation relaxation and emission spectrum of Ce ions in $(Gd_xY_{1-x})_3Al_2Ga_3O_{12}$: Ce scintillators, J. Lumin. 242, (2022), 118590.

[66] G. Tamulaitis, S. Nargelas, M. Korjik, V. Mechinsky, Y. Talochka, A. Vaitkevicius, A. Vasil'ev, Transient optical absorption as a powerful tool for engineering of lead tungstate scintillators towards faster response, J. Materials Chemistry C, 10, (2022), 9521, DOI: 10.1039/d2tc01450e.

[67] Eljen Technology: https://eljentechnology.com/products/plastic-scintillators

[68] JW. Cates et al., "Improved single photon time resolution for analog SiPMs with front end readout that reduces influence of electronic noise", Phys. Med. Biol. 63 (2018) 185022 (11pp).

[69] S. Gundacker et al, "High-frequency SiPM readout advances measured coincidence time resolution limits in TOF-PET", *Phys. Med. Biol.*, **64,** 055012, (2019). https://iopscience.iop.org/article/10.1088/1361-6560/aafd52.

[70] Z. Meng, B. Mahler et al., "Perspectives for CdSe/CdS Spherical Quantum Wells as Rapid-Response Nano-Scintillators", *Nanoscale* **2021**, *13* (46), 19578–19586

[71] Z. Meng, B. Mahler et al., "Perspective on the scintillating response of CdSe based nanoplatelets heterostructures", submitted to Material Advances (RSC)

[72] R.M. Turtos et al, "On the use of CdSe scintillating nanoplatelets as time tagger for high-energy gamma detection", *npj 2D Mater Appl* **3,** 37 (2019). https://doi.org/10.1038/s41699-019-0120-8

[73] S. Christodoulou et al., "Chlorine-induced Thickness Control in CdSe Nanoplatelets", *Nano Lett. 2018, 18, 10, 6248–6254*

[74] A. Di Giacomo et al., "Colloidal Synthesis of Laterally Confined Blue-Emitting 3.5 Monolayer CdSe Nanoplatelets", *Chem. Mater. 2020, 32, 21, 9260–9267. Publication Date:October 21, 2020*

[75] K. Tomanova et al., "On the structure, synthesis and characterization of ultrafast blue-emitting $CsPbBr_3$ nanoplatelets", *APL Materials, January 2019, American Institute of Physics, DOI: 10.1063/1.5079300.*

[76] C. Rodà, M. Zafallon et al., "Understanding Thermal and A-Thermal Trapping Processes in Lead Halide Perovskites Towards Effective Radiation Detection Schemes", *Advanced Functional Materials 31(43):2104879, DOI: 10.1002/adfm 2104879.*

[77] K. Decka et al., "Scintillation Response Enhancement in Nanocrystalline Lead Halide Perovskite Thin Films on Scintillating Wafers", *Nanomaterials, Vol. 12, Issue 1.*

[78] J. Perego, A. Vedda et al., "Highly luminescent scintillating hetero-ligand MOF nanocrystals with engineered Stokes shift for photonic applications", *Nature communications, **13**, Article number: 3504 (2022.)*

[79] H. Burešová et al., "Preparation and luminescence properties of ZnO:Ga", *Optics Express, 2016. DOI: 10.1364/oe.24.015289.*

[80] K. Děcká et al.," Timing performance of lead halide perovskite nanoscintillators embedded in a polystyrene matrix" *J. Mater. Chem. C*, 2022, Advance Article DOI https://doi.org/10.1039/D2TC02060B

[81] T. Hubacek et al., "Advancement toward ultra-thick and bright InGaN/GaN structures with a high number of QWs", Cryst. Eng. Comm., 2019, 21, 35

[82] Park, H et al. "Silicon photomultiplier signal readout and multiplexing techniques for positron emission tomography: a review." Biomedical Engineering Letters (2022): 1-21.
[83] Gola, A et al. (2019). "NUV-Sensitive Silicon Photomultiplier Technologies Developed at Fondazione Bruno Kessler." *Sensors*, *19*(2), 308
[84] Nemallapudi, M. V., et al. "Single photon time resolution of state of the art SiPMs." *Journal of Instrumentation* 11.10 (2016): P10016
[85] S. I. Kwon et al., Improving SiPM Performance for Time-of-Flight (TOF) PET Detectors Based on Bismuth Germanate (BGO), *2021 IEEE Nuclear Science Symposium (NSS) and Medical Imaging Conference (MIC), Tokyo, Japan, 2021.*
[86] S. Enoch, A.Gola , P. Lecoq, A. Rivetti , Design considerations for a new generation of SiPMs with unprecedented timing resolution , 2021 JINST 16 P02019
[87] E. Mikheeva et al., CMOS compatible all dielectric metalens for improving pixel photodetector arrays, APL Photonics **5**, 116105 (2020); https://doi.org/10.1063/5.0022162
[88] S. Uenoyama & R. Ota, (2021). 40× 40 "Metalens Array for Improved Silicon Photomultiplier Performance". *ACS Photonics, 8(6), 1548-1555.*
[89] S. Uenoyama & R. Ota, "Monolithic integration of Metalens in Silicon Photomultiplier for Improved Photodetection Efficiency", *Adv. Optical Mater. 2022, 2102707.*
[90] F. Gramuglia et al., "Sub-10ps Minimum Ionizing Particle Detection With Geiger-Mode APDs", *Front. Phys., 11 May 2022 Sec. High-Energy and Astroparticle Physics. DOI : 10.3389/fphy.2022.849237.*
[91] L. Paolozzi et al., "Test beam measurement of the first prototype of the fast silicon pixel monolithic detector for the TT-PET project". *Journal of Instrumentation, 13(04), P04015, 2018.*
[92] See for example summary table III in V. Nadig et al., "Investigation of the Power Consumption of the PETsys TOFPET2 ASIC", in *IEEE TRPMS, vol. 4, no. 3, pp. 378-388, May 2020.*
[93] www.petsyselectronics.com
[94] R. Bugalho et al., "Experimental characterization of the TOFPET2 ASIC", *2019 JINST 14 P03029.*
[95] M. Krake et al., "Power-efficient high-frequency readout concepts of SiPMs for TOF-PET and HEP", *Nuclear Instruments and Methods in Physics Research Section A, Volume 1039, 2022, 167032, ISSN 0168-9002, https://doi.org/10.1016/j.nima.2022.167032.*
[96] E. Albuquerque et al., "Results with the TOFHIR2X version of the front-end ASIC of the CMS Barrel Timing Layer", *Conference Records of IEEE Nuclear Science Symposium and Medical Imaging Conference, 2021.*
[97] The CMS Collaboration, "Technical Design Report of the MIP Timing Detector for the CMS Phase-2 Upgrade", *15 Mar 2019, CERN-LHCC-2019-003; CMS-TDR-020.*
[98] A. Gola, C. Piemonte and A. Tarolli, "Analog Circuit for Timing Measurements With Large Area SiPMs Coupled to LYSO Crystals," *IEEE Trans. Nucl. Sc*., vol. 60, no. 2, pp. 1296-1302, April 2013.
[99] L. Barrientos et al., in preparation for Phys. Med. Biol.
[100] S. Gomez et al., "FastIC: A highly configurable ASIC for Fast Timing Applications", *2021 IEEE Nuclear Science Symposium (NSS) and Medical Imaging Conference (MIC), Tokyo, Japan, 2021.*
[101] R. Viegas et al., under review in Rad. Phys. Chem.
[102] Sun Il Kwon, R. Ota, E. Berg, S. Cherry, "Cross-sectional image generation and post processing in reconstruction-free direct positron emission imaging (dPEI)", *presented at the FTMI workshop **2022.***
[103] Indranil Pan, S Palmer, A Batchvaraov, R Klapaukh, L Mason, R Craster, O Matar, "Fast prototyping of medical imaging detectors using AI methods", *presented at the FTMI workshop **2022.***
[104] J. Nuyts, M. Defrise, S. Gundacker, E. Roncali, P. lecoq, , "The SNR of positron emission data with Gaussian and non-Gaussian time-of-flight kernels, with application to prompt photon coincidence", *IEEE Trans Med Imaging*, 2022, doi: 10.1109/TMI.2022.3225433.
[105] J. Nuyts, E. Roncali, C. Trigila, M. Defrise, S. Gundacker, P. Lecoq, "The influence of the number of Cherenkov photons on the timing resolution of a BGO PET detector", *presented at the FTMI workshop **2022.***
[106] N. Efthimiou *et al*., "TOF-PET Image Reconstruction With Multiple Timing Kernels Applied on Cherenkov Radiation in BGO," in *IEEE Transactions on Radiation and Plasma Medical Sciences*, *vol. 5, no. 5, pp. 703-711, Sept. 2021.*.
[107] P. Mohr et al., "Image reconstruction analysis for positron emission tomography with heterostructured scintillators", IEEE Transactions on Radiation and Plasma Medical Sciences, https://doi.org/10.1109/TRPMS.2022.3208615
[108] Nicola Belcari, E Ciarrocchi, MG Bisogni, G Sportelli, M Morrocchi, P Carra, V Rosso, "Pushing the limits of high resolution detectors based on monolithic scintillators for fast timing in PET with an AI-boosted 4D positioning algorithm", *presented at the FTMI workshop **2022.***
[109] R. Ota, S Il Kwon, E Berg *et al.* "Direct positron emission imaging: ultra-fast timing enables reconstruction-free imaging." *arXiv preprint* arXiv:2105.05805 (2021).
[110] Stefaan Vandenberghe, M Stockhoff, J Maebe, F-M Muller, M Abi Akl, R Van Holen, "The potential of AI-Deep learning for improving spatial and TOF resolution, acquisition time and scanner cost in PET", *presented at the FTMI workshop **2022.***
[111] J. Maebe, S Vandenberghe, "Convolutional networks for gamma time estimation from raw detector waveforms in monolithic PET detectors", *presented at the FTMI workshop **2022.***
[112] Roger Lecomte, M Toussaint, F Loignon-Houle, J-P Dussault, "Improving Spatial Resolution with Ultrafast TOF in PET", *presented at the FTMI workshop **2022.***
[113] M Toussaint, R Lecomte, J-P Dussault. "Improvement of Spatial Resolution With Iterative PET Reconstruction Using Ultrafast TOF." *IEEE Transactions on Radiation and Plasma Medical Sciences* 5.5 2020: 5.5, 729-737.
[114] Carra, P., Bisogni, M. G., Ciarrocchi, E., Morrocchi, M., Sportelli, G., Rosso, V., & Belcari, N. "A neural network-based algorithm for simultaneous event positioning and timestamping in monolithic scintillators". *Physics in Medicine & Biology* 2022: 67, 135001.
[115] CK Abbey, HH Barrett, "Human- and model-observer performance in ramp-spectrum noise: effects of regularization and object variability". *J Opt Soc Am A Opt Image Sci Vis*. 2001; 18(3): 473–488.
[116] A Mehranian, SD Wollenweber, MD Walker *et al*., "Deep learning–based time-of-flight (ToF) image enhancement of non-ToF PET scans", *Eur J Nucl Med Mol Imaging*, 2022, https://doi.org/10.1007/s00259-022-05824-7.